TECHNICAL UNIVERSITY OF LIBEREC
Faculty of Mechanical Engineering

Fatigue properties of H13 tool steel processed with use of Selective Laser Melting technology

Master thesis

Study programme: N2301 – Mechanical Engineering
Study branch: 2302T010 – Machines and Equipment Design

Author: **Jitenda Reddy Kondapally**
Supervisor: Ing. Jiří Šafka, Ph.D.

Liberec 2017

TECHNICKÁ UNIVERZITA V LIBERCI
Fakulta strojní

Únavové vlastnosti nástrojové oceli H13, zpracované technologií Selective laser melting

Diplomová práce

Studijní program: N2301 – Strojní inženýrství
Studijní obor: 2302T010 – Konstrukce strojů a zařízení

Autor práce: **Jitenda Reddy Kondapally**
Vedoucí práce: Ing. Jiří Šafka, Ph.D.

Liberec 2017

Technical University of Liberec
Faculty of Mechanical Engineering
Academic year: **2016/2017**

DIPLOMA THESIS ASSIGNMENT

(PROJECT, ART WORK, ART PERFORMANCE)

First name and surname:	**Jitendra Reddy Kondapally**
Study program:	**N2301 Mechanical Engineering**
Identification number:	**S15000592**
Specialization:	**Machines and Equipment Design**
Topic name:	**Fatigue properties of tool steel processed with use of Selective Laser Melting technology**
Assigning department:	**Department of Manufacturing Systems and Automation**

Rules for elaboration:

Aim of the work is experimental quantification of strain-life fatigue curves for the tool steel which was processed using Selective Laser Melting technology. Crucial part of the work is State of the Art report mapping the latest knowledge of tool steel fatigue properties and methods of fatigue testing. On the basis of the report conclusions, fatigue tests of the material will be carried out. Finally, experimental data will be compared with the fatigue curves available in the scientific literature.

1. State of the Art report mapping the latest knowledge of tool steel fatigue properties
2. Fatigue tests of as-build and annealed tool steel specimens processed via SLM technology
3. Evaluation of strain-life fatigue curves on the basis of experimental data
4. Comparison of experimental data with the data from literature
5. Assessment of the results and conclusion

Scope of graphic works:	**as required**
Scope of work report (scope of dissertation):	**60 pages**
Form of dissertation elaboration:	**printed/electronical**
Language of dissertation elaboration:	**English**

List of specialized literature:

[1] DOWLING, N. E. Mechanical behavior of materials. 4th ed., International ed. Harlow: Pearson Education, 2011. ISBN 978-0-273-76455-7
[2] DONGDONG, G. Laser additive manufacturing of high-performance materials. Berlin: Springer, 2015. ISBN 978-3-662-46088-7.
[3] STEEN, W. M. a J. MAZUMDER. Laser Material Processing. 4th Edition. London: Springer, 2010. ISBN 978-1-84996-061-8.
[4] STEPHENS, R. I., A. FATEMI, R. S. STEPHENS a H. O. FUCHS. Metal fatigue in engineering. Second edition. New York: Wiley-Interscience, 2001. ISBN 0-471-51059-9

Tutor for dissertation:	**Ing. Jiří Šafka, Ph.D.** Department of Manufacturing Systems and Automation
Date of dissertation assignment:	**1 November 2016**
Date of dissertation submission:	**1 February 2018**

prof. Dr. Ing. Petr Lenfeld
Dean

L.S.

Ing. Petr Zelený, Ph.D.
Head of Department

Liberec, dated: 1 November 2016

Declaration

I hereby certify that I have been informed that Act 121/2000, the Copyright Act of the Czech Republic, namely Section 60, School-work, applies to my master thesis in full scope. I acknowledge that the Technical University of Liberec (TUL) does not infringe my copyrights by using my master thesis for TUL's internal purposes.

I am aware of my obligation to inform TUL on having used or licensed to use my master thesis in which event TUL may require compensation of costs incurred in creating the work at up to their actual amount.

I have written my master thesis myself using literature listed therein and consulting it with my supervisor and my tutor.

I hereby also declare that the hard copy of my master thesis is identical with its electronic form as saved at the IS STAG portal.

Date: 16-05-2017

Signature: K. Jitendra Reddy

Abstrakt

Tato diplomová práce se zabývá studií mikrostruktury a únavových vlastností nástrojové oceli AISI H13, která je zpracována technologií Selective laser melting. Vlastnosti této nástrojové oceli ji předurčují k použití v oblasti výroby forem na tváření kovů a plastů, zejména pak v oblasti tlakového lití hliníkových slitin. Tyto formy jsou vystaveny opakovanému cyklickému namáhání vlivem pracovního cyklu forem a práce má prokázat vhodnost "tisknutého" materiálu pro danou aplikaci. V současné době se jedná o aktuální a potřebné téma. Mikrostruktura je studována ve stavu přímo po stavbě a ve stavu po žíhání na odstranění vnitřního pnutí. V hlavní části práce je experimentálně odvozena únavová křivka deformace daného materiálu a výsledné hodnoty jsou porovnány s literaturou.

Klíčová slova: Selective Laser Melting, SLM, Aditivní výroba, Nástrojová ocel.

Abstract

This thesis work presents the study of microstructure and fatigue properties of AISI H13 tool steel processed by Selective Laser Melting technology. The specific application of Selective Laser Melting Technology is used for making die casting and forging dies from H13 tool steel, which are subjected to cyclic loading during the operations. Moreover, the acceptance of SLM is limited due to the lack of knowledge on operational behavior of the parts. Microstructure is studied in as-built and heat treated condition in order to evaluate impact of stress-relief annealing to properties of the material. Strain-life fatigue tests are performed on SLM-printed and annealed specimens and the results are compared with properties of H13 tool steel manufactured by conventional methods.

Keywords: Selective Laser Melting, SLM, Additive Manufacturing, Tool steel.

Number of pages: 69
Number of appendices: 3
Number of figures: 49
Number of tables: 12
Number of graphs: 2

Acknowledgements

The are the words I always believe in Guru Brahma, Guru Vishnu, Guru devo Maheshwara, Guru sakshat, param Brahma, tasmai shri guravay namah which gives the meaning that teacher is god.

Foremost, I would like to express my sincere gratitude to my supervisor Ing. Jiří Šafka, Ph.D. for the continuous support of my thesis work, for there patience, motivation, enthusiasm, and immense knowledge. Specially, I would like to thanks to my Professor Ing. Michal Ackermann, Ph.D. for great support and guidance throughout my work and made it to finish on time and i think Thanks is very small word for his support. I would also like to thank COMTES FHT company for their help in thesis work.

Besides my advisers, I would like to especially thank prof. Ing. Přemysl Pokorný, CSc. and Ing. Petr Zelený, Ph.D. for there suggestions to improve my professional skills throughout my study. I would also like to thank Ivana Pekařová for her care, which made my study in Czech Republic smooth.

First thank to your teacher and then to family because parents give the birth but teacher turns you to be knowledgeable – these are word taught by my parents. I would like to thank my parents, Kondapally Timo Sankar Reddy and Sujatha, for giving birth to me at the first place and supporting me spiritually throughout my life. I need to thank Kondapally Timo Sankar Reddy, my father, who taught me the value of hard work and an education. Without him, I may never have gotten to where I am today.

Contents

List of Figures

List of Tables

List of abbreviations

AM	Additive Manufacturing
SLM	Selective Laser Melting Technology
3D	Three Dimensional
SL	Stereolithography
FDM	Fused deposition modeling
SGC	Solid ground curing
LOM	Laminated Object Manufacturing
SLS	Selective Laser Sintering
LEAP	Type of engine used for the aircraft
CAD	Computer Aided Design
U.K	United Kingdom

List of symbols

Symbol	Decsription	Unit
b	Fatigue strength exponent	-
c	Fatigue ductility exponent	-
d	Diameter	mm
E	Young's Modulus	N/mm^2
h	Hatch Angle	θ
l	Length	mm
P	Laser power	W
R	Stress Ratio	-
t	Layer Thickness	mm
v	Scanning Speed	$\frac{mm}{s}$
$\sigma_f^{'}$	Fatigue Strength Coefficient	
σ_a	Stress Amplitude	MPa
σ_r	Stress Range	MPa
σ_m	Mean Stress	MPa
σ_{max}	Maximum stress	MPa
σ_{min}	Minimum Stress	MPa
σ_{comp}	Compressive Stress	MPa
σ_{ten}	Tensile Stress	MPa
N_f	Number of cycles	-
$\varepsilon_f^{'}$	Fatigue ductility Coefficient	-
ε_a	Total Strain	-
ε_e	Elastic Strain	-
ε_p	Plastic Strain	-

1 Introduction

Additive Manufacturing (AM) is the process that enable the complex 3D parts to be manufactured by adding material layer by layer rather that by conventional material subtracting method. Such approach dramatically reduces the material waste and building time and cost of prototypes. This diploma thesis deals with one of the youngest member of AM family – Selective Laser Melting (SLM) technology. Using SLM process, it is almost possible to get the full density metal parts like in the case of parts produced by conventional methods. In the present days, many manufacturers are showing their interest to use this technology as a tool for manufacturing not only metal prototypes but also end-use parts.

Topic of my thesis work arose from research activities in Laboratory of Rapid Prototyping at the The Institute for Nanomaterials, Advanced Technology and Innovation at Technical University of Liberec. In this laboratory, researchers are concentrating on manufacturing parts with use of SLM technology for the industrial applications. To achieve this, a research was done to show that parts produced by Selective Laser Melting technology can substitute the parts which are manufactured by conventional processes. In order to prove the practical applicability of SLM printed parts, they have done many tests to evaluate their final mechanical properties such as tensile test, hardness test and surface roughness test. Results from their research work help them to built the parts for the industrial application with guaranteed properties.

One of the most vital topics of the laboratory is production of complex pressure casting molds with conformal cooling for both plastic and aluminum products. These types of molds have to be made from such a material which is capable to sustain high mechanical and thermal loads. For SLM process, there are several types of metal powders which can be used for this purpose. One of the most convenient materials is AISI H13 (DIN 1.2344) tool steel. This type of steel shows good mechanical properties even at elevated temperatures and it is capable to sustain high frictional forces during high pressure casting of aluminum.

From the SLM processing point of view, it is a real challenge to manufacture parts from H13 tool steel without any defects. Point melting and very fast solidification of the material during SLM process leads to introduction of high internal stresses. By this reason, previous work of the laboratory was aimed to development of building strategy and basic mechanical tests were carried out. Taking into account that mold cavities are subjected to high number of loading cycles, it was decided to study the fatigue properties of H13 tool steel processed by SLM process.

1.1 Research aim and methodology

The primary aim of this investigation is understanding of fatigue properties of H13 tool steel processed by SLM technology. This includes evaluation of both material properties and process parameters. The knowledge can be used for designing of the SLM-printed parts in order to prevent its premature failure due to fatigue processes.

All the samples were produced in the Laboratory of Rapid Prototyping at the The Institute for Nanomaterials, Advanced Technology and Innovation at Technical University of Liberec using SLM 280^{HL} machine from German manufacturer SLM Solutions AG.

1.2 Outline

My diploma thesis is divided into two major parts – theoretical (Chapters 2 to 4) which maps current state-of-the-art and experimental (Chapters 5 and 6).

In the initial chapter that follow (Chapter 2), the details of the SLM process are discussed together with different key parameters and side effect in SLM. This helps the reader to understand the effects of processing parameters on mechanical properties. Chapter 3 provides information about basics in fatigue and different approaches for measuring the fatigue life. More detail is given to strain-life fatigue approach because this approach is used for testing. Chapter 4 is dedicated to explanation of H13 tool steel which is used as a testing material. In this chapter, we can see the chemical composition of H13 tool steel for both conventional method and SLM method. Moreover, the mechanical properties of H13 tool steel which is processed by conventional methods is provided in the chapter.

The experimental part of the work is divided into two chapters. Chapter 5 deals with influence of current building strategy to internal structure of the specimens. Special attention is paid to overall density of the parts and influence of heat treatment. Main part of the work is contained in Chapter 6. Production process of the samples using SLM process is explained and results of both quasi-static and fatigue testing are provided. As a result, strain-life curve of the SLM–printed H13 tool steel is constructed.

2 Selective laser melting technology

2.1 Introduction

Selective laser melting (SLM) is an emerging manufacturing technology which comes under Additive manufacturing (AM) group and more specifically, it fits into the AM's Powder Bed Fusion subgroup. In SLM process, the input material is in the form of metal powder which is selectively melted using laser according to the CAD data. Same as in the case of other Powder Bed Fusion technologies, the part is surrounded by unprocessed material during its build. This chapter deals with basic properties of SLM technology, its area of application and its strong points and weak points.

2.2 Historical background

In early 1987, 3D Systems introduced the first 3D printer which works on Stereolithography (SLA) technology which uses photo-sensitivity polymer to build the part. Introduction this technology played an important role in building prototypes faster than ever before, because of unique Rapid manufacturing technique called layer by layer approach. In 1991, three more important technologies were introduced. Namely, Fused Deposition Modeling (Strasys), Solid Ground Curing (Cubital) and Laminated Object Manufacturing (Helisys) [19].

All of these unique manufacturing techniques graded interest of many researchers and manufacturers and encouraged them to develop a process which is capable of manufacturing metal parts. This goal was achieved in the year 1986 with introduction of a new technology called Selective Laser Sintering (SLS). This technology was developed by University of Texas at Austin [19]. Even though SLS technology was able to process different types of materials, it failed in producing 100% dense metal part. This effect is caused because of heating the material near to the melting temperature by the laser rather than melting it. This process creates the bounds between the powder particles which results in high porosity.

In the year 2000, new technology was introduced by the German company SLM solutions called selective laser melting technology (SLM) [16]. This technology was derived from the SLS technology and main difference is that input powder is fully melted during the process in the case of SLM. By the use of selective laser melting technology, we can produce the complex shape parts which are difficult to manufactured by conventional methods. For example, LEAP engine fuel nozzle manufactured by GE Aviation 2.1 originally consisted of assembly of 20 separate parts with com-

plex passageways. Using SLM technology in GE Aviation, the engineers were able to manufacture LEAP nozzle as single component. It is expected that by 2020 GE aviation will produce 10,000 excess parts for LEAP engines which are manufactured by SLM technology [16]. Apart from SLM and SLM technologies, there is one more technology which can produce metal parts called Electron Beam Melting (EBM) technology. In this technology, electron beam is used as source for melting the powder particle and produce 100 % dense part. EBM is mostly used for limited number of high performance materials like titanium alloys and cobalt–chromium. Moreover, EBM technology based machines are more expensive compared to SLM and SLS machines.

Figure 2.1: LEAP nozzle produced by GE Aviation

2.2.1 Key manufacturers

On today's market, there are several manufacturers who provide SLS, SLM and EBM machines. Main companies together with the technology are summarized in table 2.1.

Manufacturer	Technology	Country
SLM Solutions AG	SLM	Germany
RENISHAW	SLM	U.K
ARCAM	EBM	Sweden
Concept Laser	SLM	Germany
EOS EOSINT	DSLM	Germany
Realizer	SLM	Germany
Sclaky	EBM	U.S.A

Table 2.1: Key Manufacturers

2.3 Main principle

Selective laser melting technology process starts with transferring the sliced CAD model data to SLM machine. After the data is transferred, the substrate plate is fastened to index table, which can can moved vertically in Z-axis. After precise positioning of the platform, first layer of metal powder is evenly distributed on the plate. This process take place in tightly closed chamber under controlled atmosphere. Usually, nitrogen (N_2) or argon (Ar) are used to reduce the oxygen level below 500 parts per million. Once the layer is spread evenly, 2D sliced data of the CAD geometry is fused by selective melting of the metal powder. This is done with the help of the high power laser beam. The laser beam is directed in X and Y axis by using two high frequency scanning mirrors. This process is repeated for every layer until completion of part. In the figure 2.2 the principle of the SLM process is schematically described [15].

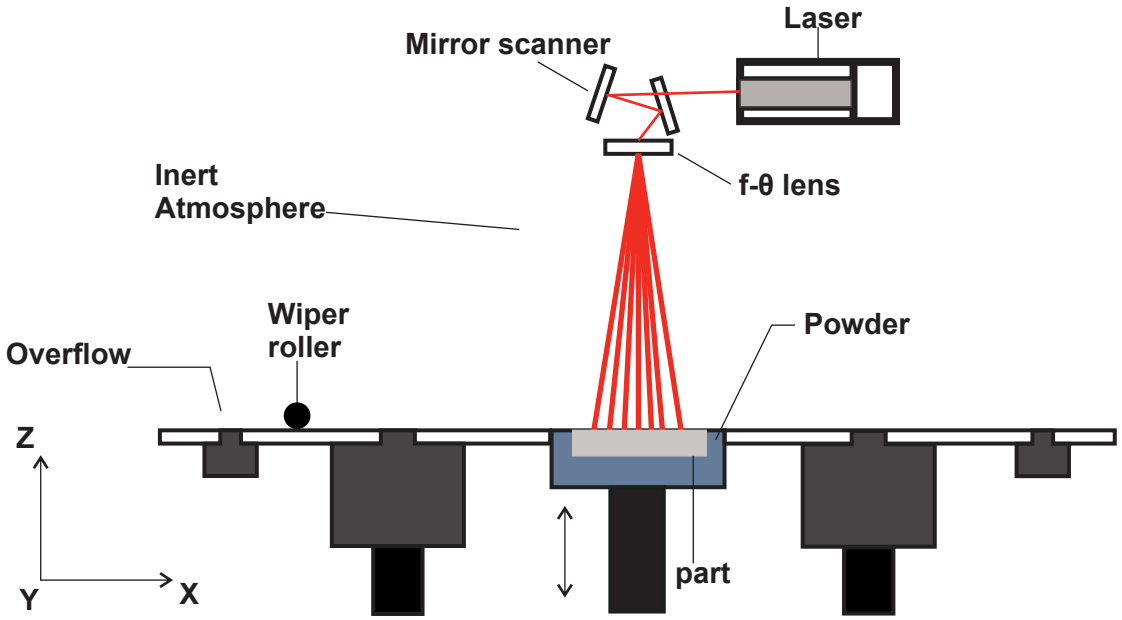

Figure 2.2: schematic view of selective laser melting cycle [15]

2.4 SLM key parameters

Among all the parameters influencing the final output when using SLM process, we can find four parameters which contribute the final quality in the most significant way. Namely, Laser power, Scanning speed, distance between neighboring laser pathways and layer thickness. The two less significant parameters – scanning strategy and hatch angle of the adjacent layers – will be discussed in this section as well

2.4.1 Scanning speed and Laser power

In order to gain the structure of the material similar to the conventional manufacturing process, scanning speed and laser power are very important parameters. There are different types of phenomena which occur during SLM process, due to improper scanning speed and laser power. The test conducted on SLM process by Hanzl et al. [7] using 316L stainless steel powder as a testing material, says that they observed different phenomena in the structure with different laser power and scanning speed as explained below.

- No melting: In this phenomenon, the energy delivered by the laser beam is not sufficient for melting of the powder, so most of the powder remain in the initial state after the process.
- Partial melting: This phenomena with medium laser power and low scanning speed ($v < 0.06\,\mathrm{m/s}$) forms a liquid phase on particle surface which bake together the unmelted particle which lead to the pores structure how in the figure 2.3 (c).
- Melting with high scanning speed: Melting with high scanning speed >0.006 m/s leads to the balling phenomena, because of insufficient scanning speed we can the structure in this phenomena in figure 2.3 (b).
- Complete melting with required scanning speed: laser energy was so great that permanent tracks of molten metal material was created. The structure of the material is similar to the conventional part which is shown in the below figure 2.3 (a)

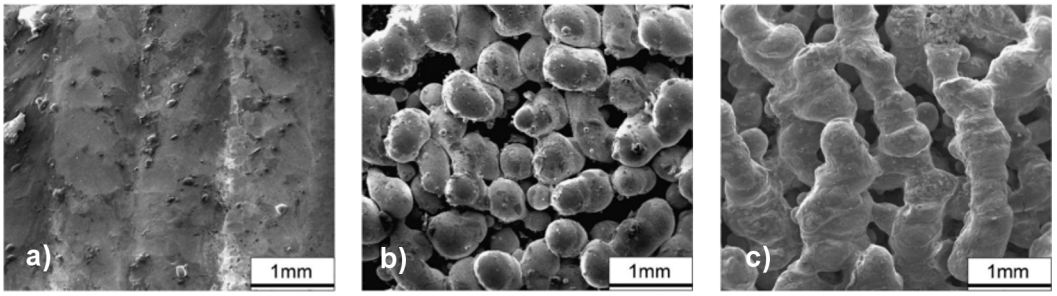

Figure 2.3: Different phenomena with different laser power and scanning speed [7]

2.4.2 Scanning strategy

Scanning strategy is able to reduce temperature gradient mechanism and it will be discussed in this section. In the figure 2.4, there are four different strategies, which explain how they are effecting the temperature gradient mechanism.

First scanning strategy scanning in X-direction results in smallest curvature in X-direction and longest in Y-direction. Similarly in line Y scanning strategy smallest in Y-direction and longest in X-direction. In the these two types of scanning strategy, we can observe that there is more time for cooling until scanning the next track, which leads to internal stress and deformation of the build part.

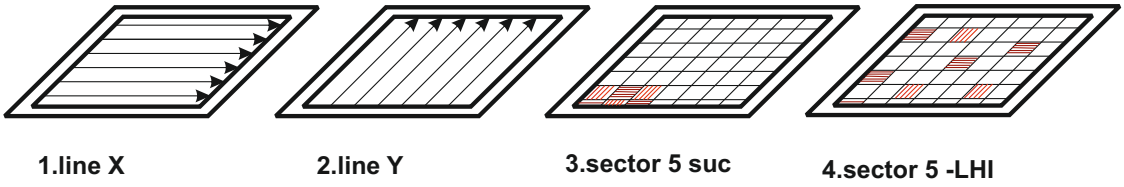

Figure 2.4: Overview of SLM scanning strategies [7]

In order to avoid this effect, entire cross section is divided into small sectors of size 5×5 mm (Figure 2.4 3. and 4.) scanning strategies, called least heat influence. In these two scanning strategies we can can observe the small curvatures in both X and Y direction which reduces the internal stress and deformation compare to line X and line Y scanning strategy [9].

2.4.3 Influence of hatching angle and distance

The hatch angle θ is defined as the angle between scanning direction on consecutive layers as shown in the figure 2.5. For example, the hatch angle $90\,^{\circ}$ means that after deposition melted row in four layers, the orientation in the next melted row is same as first layer. Anisotropy of mechanical properties is difficult to remove. This happens when improper hatch angle is selected.

Test conducted by the Hanzl using 316L material with hatch angle (105°) shows the most satisfactory mechanical properties in many applications [7]. Along with proper hatch angle proper hatch distance also influences the final output. Hatch distance is defined as the distance between two hatch lines. Improper selection of the hatch distance lead to overlapping of metal which lead to the porosity in the final part. Before selection of the hatch distance one should know the melt pool size, in order to avoid the overlapping.

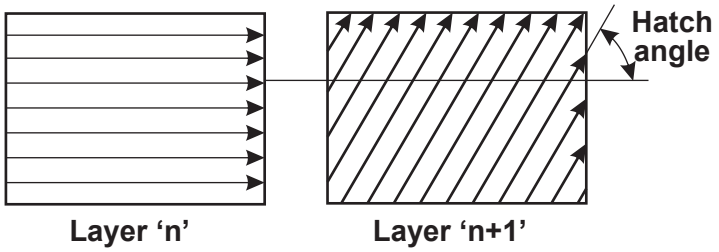

Figure 2.5: Rotation of line in neighboring planes [7]

2.4.4 Influence of Layer thickness

For different layer thickness, different laser parameters must be used. For example, if we select the 30 µm layer thickness laser should be able to melt the layer. In order to achieve this proper laser parameters must be used. Moreover, layer thickness shows its influence on surface quality, internal structure and time of production of the part.

2.4.5 Energy density function

In selective laser melting technology (SLM), laser is used as an energy source to melt the metal powder. The quality of the metal part depend on effective melting of the powder particle during laser melting, which is largely influenced by input energy into the melt pool. The laser input energy density 'E' is the function of laser power 'P', scanning speed 'v', layer thickness 't' and hatch spacing 'h'. If the laser energy is insufficient, it leads to the high porosity, lack of fusion between the layers and low mechanical properties. Excess laser energy leads to the balling effect and vaporization effect which will be explained in the following section [12].

$$E = \frac{P}{h.v.t} \tag{2.1}$$

- E = energy density ($\frac{J}{mm^3}$)
- P = laser power (W)
- v = scanning speed ($\frac{mm}{s}$)
- t = layer thickness (mm)
- h = hatch spacing (mm)

2.5 Side effects of selective laser melting technology

2.5.1 Thermal deformations in SLM process

Selective laser melting technology is similar to welding process. Moreover in SLM, welds take place in fine scale compare to commercial welding with melt pool dimension 10^{-1} mm^3. In the below figure 2.6 we can see the model of the melt pool which is taken from the work of the vrancken [18]. In addition, due to solidification and shrinkage of the melt pool the metallurgical effects on the heat affected zone leads to the residual stress in the manufactured part. Residual stresses are one of the major drawback in selective laser melting technology which reduce the mechanical properties of the printed part [8].

The residual thermal stress in SLM process causes part to crack or delaminate from the base plate. Simple example as show in figure 2.7 M2 HSS part produced in SLM process, Where the cracks caused due to high thermal stress. There are two different phenomenons lead to thermal stress in SLM process. [8].

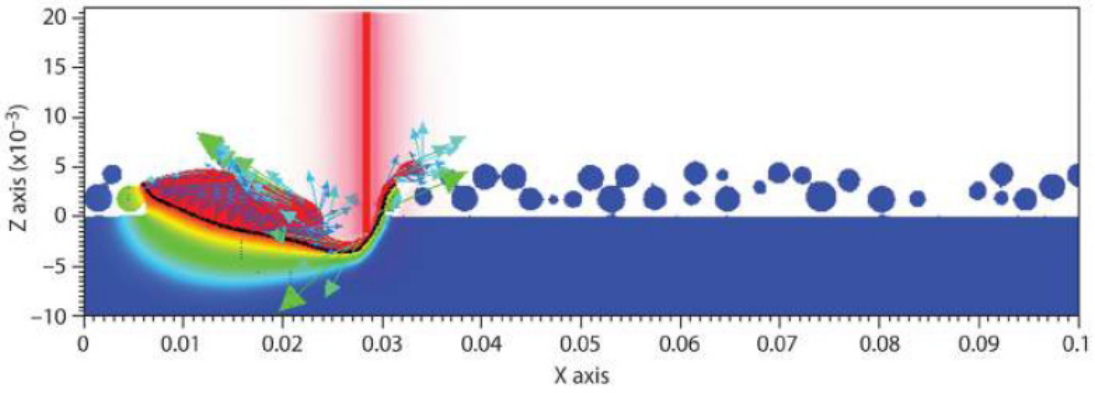

Figure 2.6: Model of the melt pool [18]

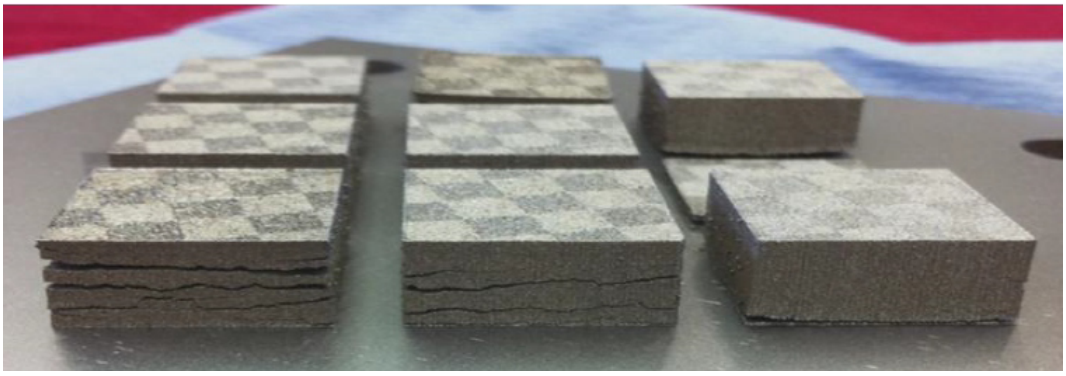

Figure 2.7: Cracks due to residual stress in M2 HSS part[8]

The first phenomena is also called as temperature gradient mechanism generally used for bending of metal sheets. Due to high temperatures metal powder is converted to molten metal which try to expand, and this expansion is restricted by cool solidified layer which is underneath. This induce a compressive stress on the upper layers of the substrate may rise above the yield strength of the material, and causes plastic upsetting on the layers. Those residual stress induces cracks in the part [8].

The second phenomena when the molten metal is in cooling phase the material tends to shrink, this is restricted by the previously solidified layers underneath the molten metal. Thus induces tensile stress on the upper layer and compressive stress in below layers. The figure 2.8 shows the both phenomena. They are different methods to avoid the cracks in the build part as we seen in the figure 2.7, some follow the pre-heating module and some follow different scanning strategy to avoid crack free part. In the below figure 2.9 we can see the pre-heated equipment which is arranged under the base plate of SLM machine and also we can see the result of the pre-heating equipment in the figure 2.10 [8, 18, 16] .

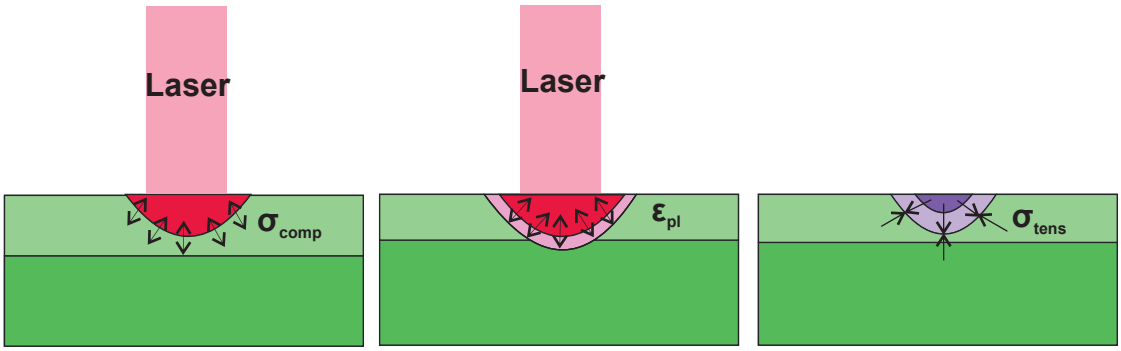

Figure 2.8: Temperature gradient mechanism [8]

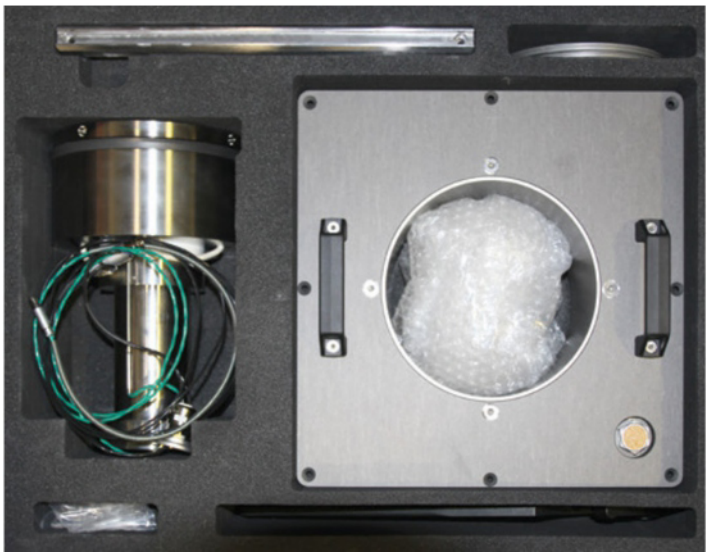

Figure 2.9: Schematic overview of pre-heating module

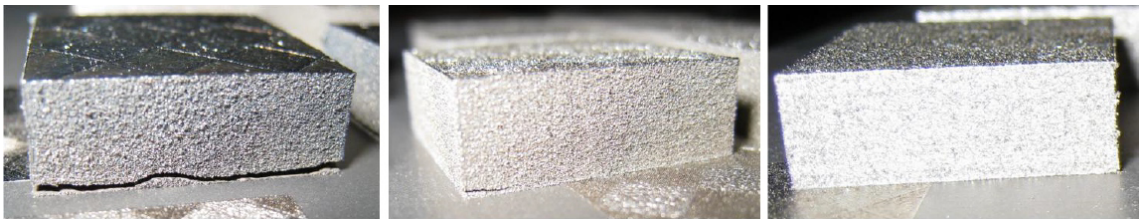

Figure 2.10: M2hss part produced with pre-heating module with 90 °C (left), 150 °C(middle), 200 °C(right) [8]

2.5.2 Balling effect

Balling or Wettability is also one of the side effect in selective laser melting technology(SLM). We can observe this phenomenon, when the molten metal is unable to wet the underlying substrate due to surface tension which tends to spheroidise the liquid. Which results in poor surface finish and low density component.

We can observe this phenomenon by taking a small example, let us consider a flat uniform base plate is in contact with non-reactive liquid in the presence of vapor. If the liquid metal dose not cover the entire solid, liquid metal interact with the solid surface at an angleθ that correspond to minimum of total free energy of the system is shown in the below figure. The value of θ accept the classical equation of young's(1804). Since laser interaction with the metal is very short in order of magnitude of milliseconds [9].

In practical situation molten pool is created by the fast moving laser spot, can be approximated by the half of the cylinder. Therefore additional reduction of surface free energy appears. When the total surface of the molten pool is larger than the sphere with same volume results in balling effect. The laser power should be selected in such a way that length to the diameter ratio should be as small as possible, to avoid the balling effect. The formula has been explained in the figure 2.11 [9].

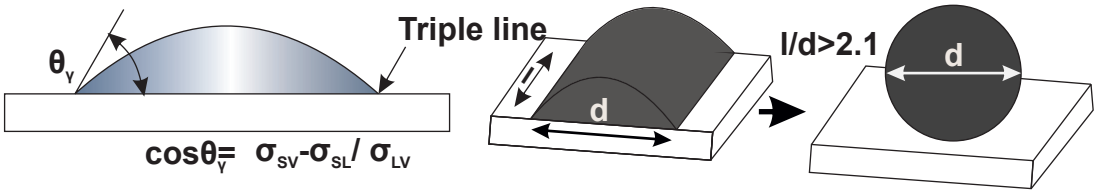

Figure 2.11: Balling effect [9]

2.5.3 Vaporization Effect

During the laser melting the metal powder temperature of the exposed powder particle exceed the melting temperature, which causes the metal powder to evaporate. When this evaporation occurs particle expands and create recoil pressure on the melt pool. While low recoiling pressure facilitate flattening the melt pool, high pressure causes metal removal by expulsion. If the intensities further increased vapor interact with laser radiation becomes ionized and form the plasma [9].

The evaporization effect can be observed by running the laser in pulsed mode, with peak intensities up to 2×10^3 W/mm^2 and the balling effect is absent and density of the solid layer is improved. This lead to high surface quality and high strength in the part. In order to achieve this the above parameters are very important, because those parameters are influencing the final part mechanical properties [9].

2.6 Advantages and Disadvantages

The Advantages of SLM Technologies are explained below

- High Quality metal parts with 100 percent density up on requirement.
- Applicable to wide range of metals like tool steel, titanium, aluminum, cobalt-chrome and nonferrous metals
- High dimensional accuracy can be achieved
- Able to produce very complex geometries.

The disadvantages of SLM technologies are.

- Occupy more space in Lab
- High power consumption because of laser and relatively slow process
- Unable to produce large components

2.7 Applications

- Aerospace and Biomedical industry
- Manufacturing of inserts for tools
- In making molds for aluminum alloys
- Building the functional prototypes

3 Fatigue of materials

3.1 Introduction

The term fatigue is taken from the human reaction of 'tiredness' due to a repetitive work. In the early 1830, fatigue failure was observed in railroad industry in Europe and United Kingdom. The engineers observed the frequent failure of railroad axle shoulders. First, they thought that the notch in sharp corner of the axle is the main reason of failure. Unfortunately, removing the notches lead only to postponing the problem and the same type of fracture occurred on about 90% of mechanical failures. In the year 1837, first paper was published on the fatigue that co-relates between cyclic loading and durability of metals, but officially the term fatigue was used in the book of mechanics by Jean-Victor Poncelet in 1839 who worked in designing of cast iron axles for mill wheel [17].

In the year 1842, one of the worst rail disaster occurred near Versailles in France because of the failure of locomotive axle. Engineer from British railways William John Macquorn Rankine showed the brittle fracture across the diameter. August Wöhler was the first man who investigated failure of the locomotive axle by cyclic loading in 1860–1870. He introduced the method of testing the locomotive axles by rotation bending fatigue test as shown in the figure 3.1. Using this type of fatigue testing setup, fully reversed bending stress is introduced into the specimen and cycles to failure are counted under specified value of load. The pioneer work of August Wöhler lead to the development of so-called Stress-life (S-N) diagram for estimating the fatigue life and the endurance limit of the material. These two terms will be explained later in this section.

In the year 1886, John Bauschinger gave the first paper about the stress-strain behavior of metals. By the end of 19^{th} century, Gerber and Goodman investigated the influence of mean stress on fatigue parameters. Based on these theories, designers started designing and implementing the fatigue analysis, by which they can predict the life of the product better that ever before. In the beginning of 20^{th} century, J.A Ewing demonstrated the origin of fatigue failure in microscopic cracks [17].

3.2 Fatigue Damage Mechanism

Fatigue process occur because of the cyclic loading which results in premature failure of the given part. When the part is subjected to cyclic loading, plastic deformation occur at high stress site. This deformation leads to permanent damage of the compo-

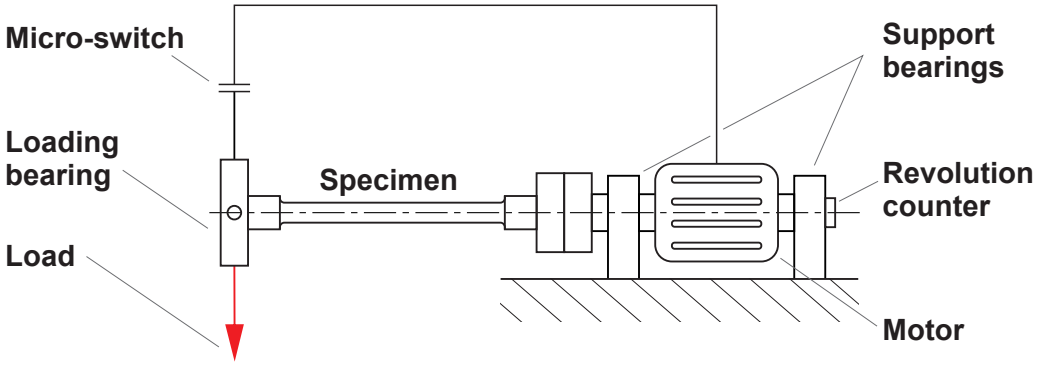

Figure 3.1: Schematic diagram of rotating–bending fatigue test

nent and development of cracks. As the component experiences more cyclic loading, length of the crack grows which eventually leads to the failure. We can observe that fatigue process involves three steps, specifically *crack initiation*, *crack propagation* and *failure*.

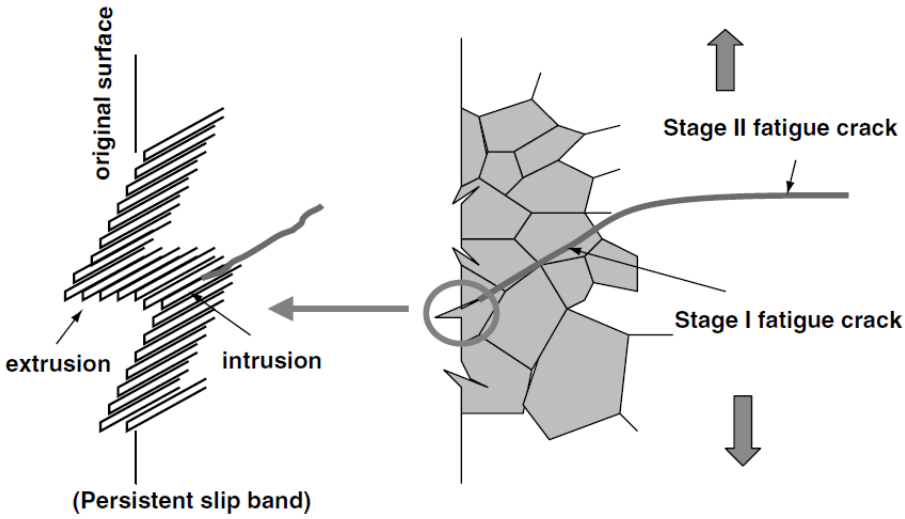

Figure 3.2: Fatigue process under cyclic tensile loading [10]

By using the figure 3.2 we can explain the mechanism in better way. In the figure, we can see that crack initiation is observed in the high stress concentration site in persistent slip band. The next step is divided into two stages: In stage 1, crack propagation is very short, specifically across finite couple of grains on the local maximum shear stress plane. In this stage, crack tip plasticity generally depends on the characteristics of the slip, grain size and stress level. Stage 2 refers to long crack propagation normal to the principle tensile stress plane and locally in direction of maximum shear stress [10].

3.3 Fractography of fatigue surface

In the figure 3.3 we can see the fracture surface of component subjected to fatigue loading. First and foremost we can observe the crack nucleation site or crack initiation site followed by two different types of cracks termed as *benchmarks* and *striation*. Both of these give the information about position of the crack tip at some point of time. Moreover they appears as concentric ridges, which expand from the crack initiation site in a circular or semi circular patterns.

Benchmarks are of macroscopic dimensions that can be viewed by unaided eye. Generally we can observe this type of benchmarks mainly in the parts subjected to interrupted loadings – for example in machines which operates only few hours a day. Each benchmark represent crack growth period. On the other hand, second type of cracks, striations are part of benchmarks. The striation represent advancement of crack during single load cycle. Therefore, one benchmark contains millions of striations. [3].

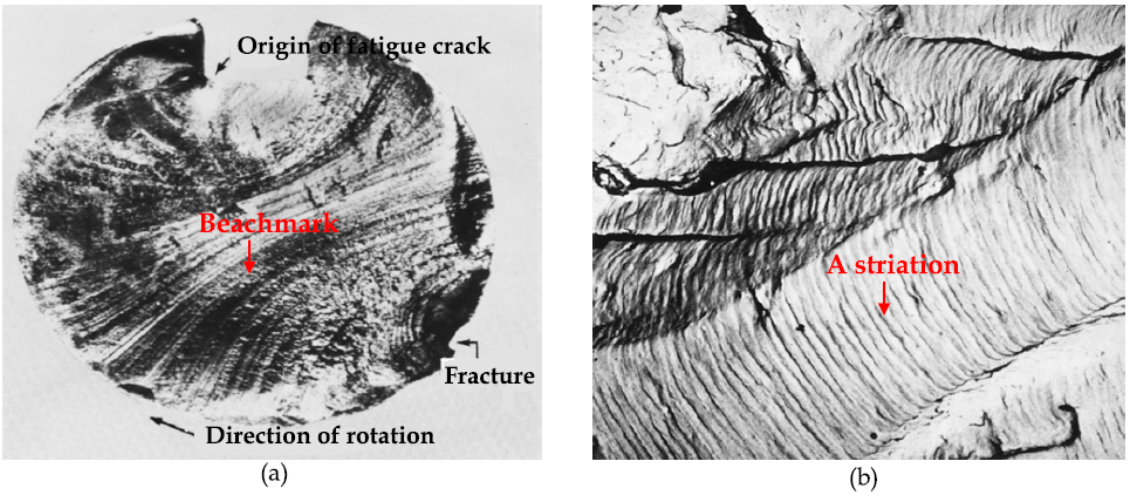

Figure 3.3: Fatigue fracture surface of steel shaft [3]

3.4 Types of cycles

In the the real world applications, parts are subjected to different type of loadings and it can be stated that about 98% of parts are subjected to completely random (stochastic) type of loading [1]. Basic parameters of the loading can be easily understood by simple loading patterns like the sinusoidal waves. The terminology which describe magnitude of loading cycle are maximum stress level σ_{max}, minimum stress level σ_{min}, mean stress of the cycle σ_m and amplitude of the cycle σ_a 3.4. [10, 17].

$$\sigma_r = \sigma_{max} - \sigma_{min} \tag{3.1}$$

$$\sigma_m = \frac{\sigma_{max} + \sigma_{min}}{2} \tag{3.2}$$

$$\sigma_a = \frac{\sigma_{max} - \sigma_{min}}{2} \tag{3.3}$$

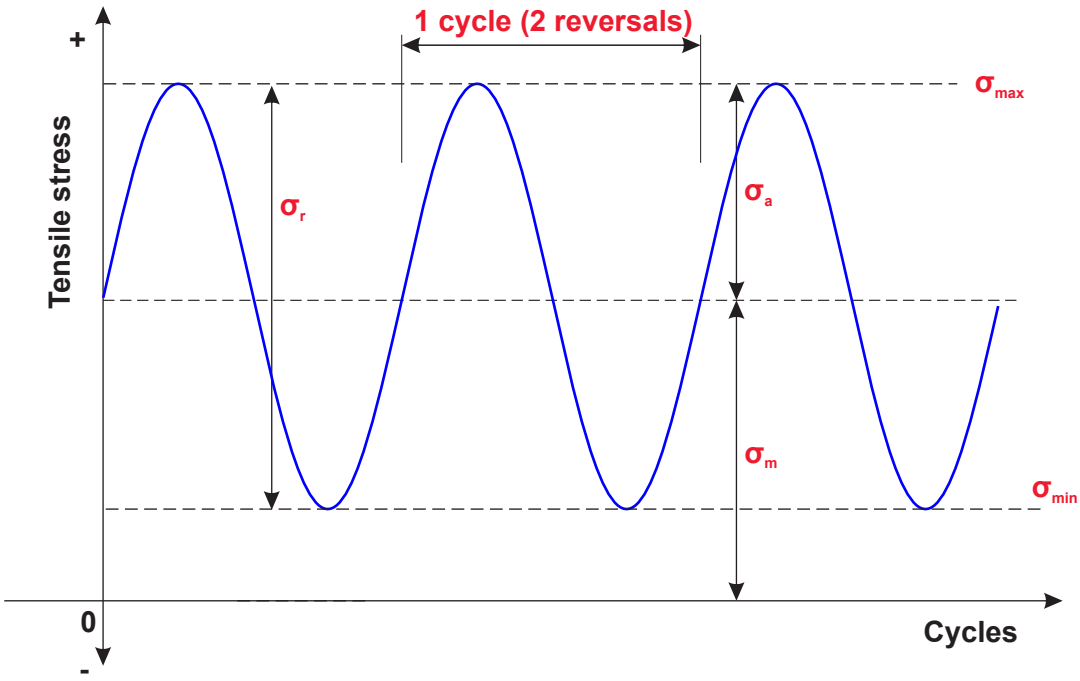

Figure 3.4: Purely tensile stress cycle

Another two quantities which are commonly used for characterization of loading cycle are stress ratio R and amplitude ratio A [4].

$$R = \frac{\sigma_{min}}{\sigma_{max}} \tag{3.4}$$

$$A = \frac{\sigma_a}{\sigma_m} = \frac{1+R}{1-R} \tag{3.5}$$

With respect to magnitude of the cycle parameters we can find three common types of loading:

1) Fully reversed cycle

This type of loading can be observed in the component subjected to symmetrical stress. Fully reversed cycle is most commonly used for material fatigue testing. Stress ratio of fully reversed cycle is $R = -1$, mean stress $\sigma_m = 0$ and $\sigma_{max} = -\sigma_{min}$. [10, 17].

2) Purely tensile or compressive stress cycle

In this type of cycle, mean stress is not equal to zero and the stress ratio is positive. Such loading can be observed in the components subjected to non-zero mean stress like in the case of valve stem in automobile. [10, 17].

3) Random stress cycle

Generally, we observe this type of loading in almost all industrial applications including aerospace, automotive and machines. Random loading cannot be easily evaluated due to the fact that its parameters vary with each cycle. An example of this type of cycle is shown in figure 3.5. During the first cycle, the specimen is subjected to symmetrical loading where stress ratio $R = -1$ and in next cycle we can observe fluctuation in the mean stress. [10, 17].

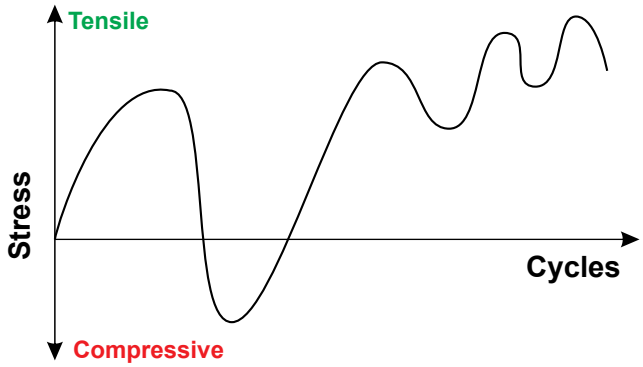

Figure 3.5: Random stress cycle

3.5 Fatigue testing methods

There are three basic models for testing and evaluation of the fatigue life which are available for design engineers. We can choose the fatigue testing model with respect to real time loading condition on the component [10, 17].

- Stress life (S-N) model
- Strain life ($\epsilon - N$) model.
- Fatigue crack growth model

3.6 Stress life (S-N) fatigue model

Stress life approach is the classical testing procedure, which is used first by the German railway engineer August Wöhler for testing the life of the railroad axle.

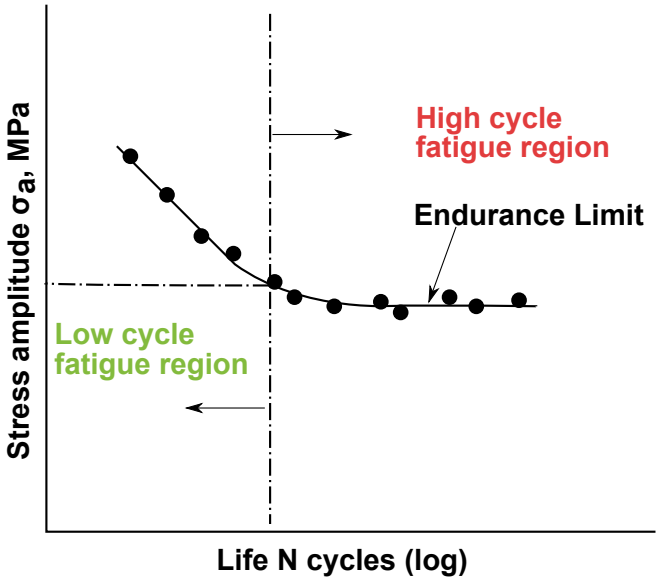

Figure 3.6: Stress-life (S-N) fatigue curve [10]

Stress-life (S-N) fatigue model has been using since mid 1850 almost more than 155 years. Conditions to use this fatigue model are summarized in below three points [10].

- Cyclic stress are the governing parameters for fatigue failure [10].
- High cycle fatigue, high number of cycles are required to the failure.
- Little plastic deformation, due to cyclic stress

Testing loads are take from the data histories, when the component is subject to the real time applications. Loads applied on the specimen are defined by constant stress range σ_r and constant stress amplitude σ_a. The magnitude of the stress range or the stress amplitude are independent variable and number cycles to the failure is dependent variable. Each stress cycle N_f is equal to 2 reversal $2N_f$ as shown in the below figure 3.6. In most of the cases test is conducted under fully reversed cyclic loading, where the mean stress σ_m is equal to zero and stress ratio is negative. [10, 17].

To generate useful data for the fatigue design using S-N approach. The test is conducted on several specimen, and the data are plotted on the log-log or semi log coordinates. Single curve used in the figure called as S-N curve or the wohler curve. which is divided in to two regions negative slop line is called as finite life region (low cycle fatigue) and horizontal line is called as infinite life region (high cycle fatigue). The point at which negative slope changes to the horizontal line is called knee of the S-N curve represent the fatigue limit [10, 17].

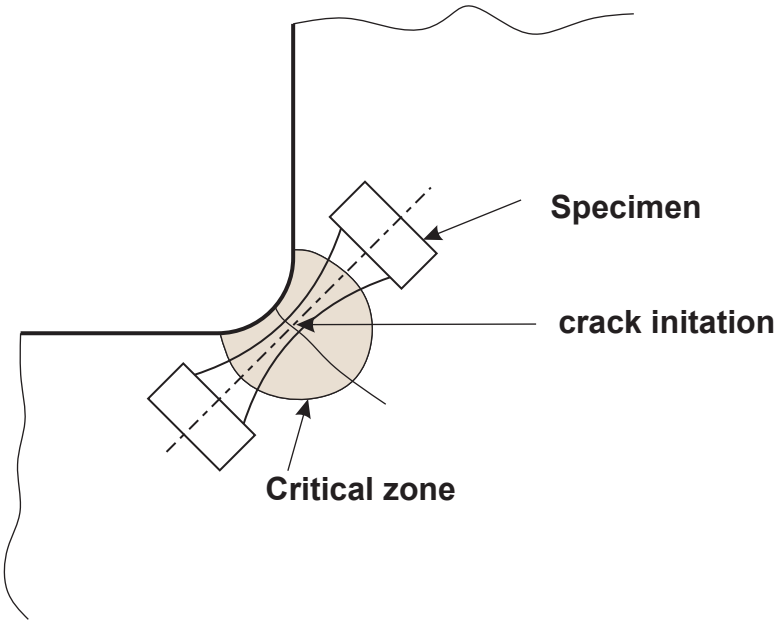

Figure 3.7: Concept of strain life approach [10]

3.7 Strain-life (ε-N) fatigue model

In the previous section, we discussed about the stress life fatigue analysis, which works well for the component which are subjected below the yield point. Even though the component are subjected to normal elastic stresses due to the presence of notches, welded joints and stress concentration areas leads to plastic deformation in this situation Strain life (ε-N) fatigue method approach is best. Strain life fatigue method developed in the year 1950. For example this method is mainly used in the aerospace industry for testing life of the components [10, 17].

Strain life fatigue relation is represented by the curve between strain and fatigue life axis as shown in the figure 3.7. The curve is generated by conducting the strain controlled axial fatigue test on cylindrical specimen according to either ASTM or ISO standards [10, 17].

3.7.1 Apparatus for the test

For testing the strain life fatigue curve we use closed loop servo hydraulic axial load frame as shown in the below figure 3.8, which is complicated when compare to the apparatus used for stress life fatigue method. In the strain life fatigue method we have to control the strain amplitude in order to achieve this we can use the extensometer for measuring the strain. which can send the feed back to the servo controllers. In order avoid the the surface scratches from the knife edges of the extensometer we use transparent tape or epoxy to cushion the attachment. Specimen Alignment is another important aspect, during the arrangement of specimen in the apparatus it should be accurate that the load cell and the specimen alignment should

be on the same axis. To the standard E606 bending strain should not exceed more than 5% of the minimum strain range during test.

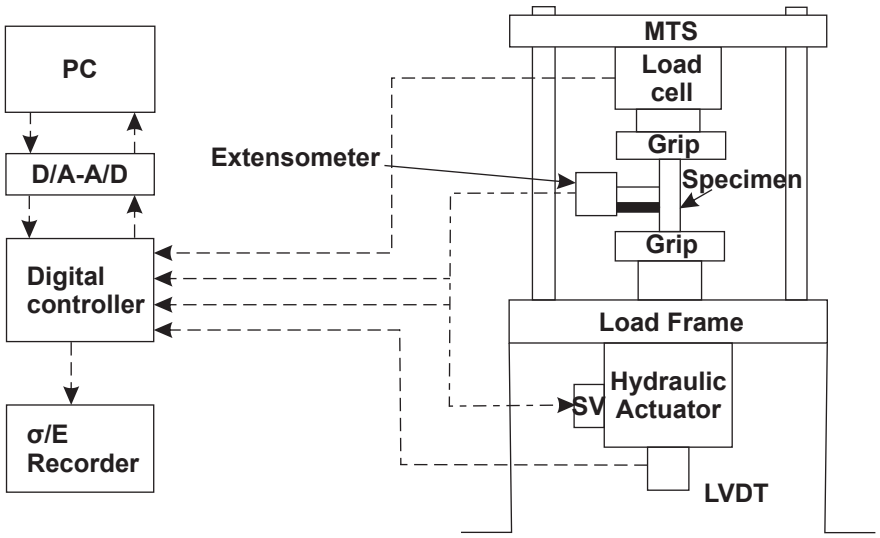

Figure 3.8: Systematic diagram for the apparatus used in strain life fatigue method [10]

3.7.2 Test method

In strain life fatigue method the specimen is prepared with good surface finish as discuss in the above section for the axial fatigue loading, with constant amplitude fully reversed cycle of strain. Steady state hysteresis loop are predominant through out the fatigue life. where the loop can be adjusted for elastic plastic strain ranges or amplitude. Number of cycle required for the failure in $(\epsilon - N)$ curve is 10 to 10^6 cycles, with the frequency of 10 HZ. If the failure reaches beyond the 10^6 cycles there is lack of plastic strain.[17, 10].

As we known the strain life fatigue method is also known as low cycle fatigue method, because most of the data obtained is between 10 to 10^5cycles. Where the data obtained in the stress life fatigue method is not suitable to get the amount of plastic strain in the material which is tested. Strain life fatigue curve is plotted on log-log scale is shown in the below figure, where $2N_f$ on the x axis gives the information about the number cycles required for the failure and y axis give the information about the strain amplitude[17, 10].

Generally there are four different failure criteria, life for the small detectable cracks, life to percent drop in the tensile load, life to fracture or decreasing in the ratio of unloading to loading module. But we follow the ASTM E606 Method for testing, according to E606 failure criteria is 50% drop in tensile load. as shown in $(\epsilon - N)$ curve in below figure total strain is divided in to two regions elastic and plastic region. Total strain at particular life N_f is sum of plastic strain and elastic strain, where elastic and plastic curves are approximated as straight line as shown in

the graph. We can observe from the graph that large strain with low life and small strain with long life. Where ϵ_f represent the plastic line with slope c in the graph and $\sigma_f^{'}$/E for the elastic line with slope b [10, 17].

$$\frac{\Delta\varepsilon}{2} = \frac{\Delta\varepsilon_e}{2} + \frac{\Delta\varepsilon_p}{2} \tag{3.6}$$

$$\frac{\Delta\varepsilon_e}{2} = \frac{\sigma_f^{'}}{E}(2N_f)^b \tag{3.7}$$

$$\frac{\Delta\varepsilon_p}{2} = \varepsilon_f^{'}(2N_f)^c \tag{3.8}$$

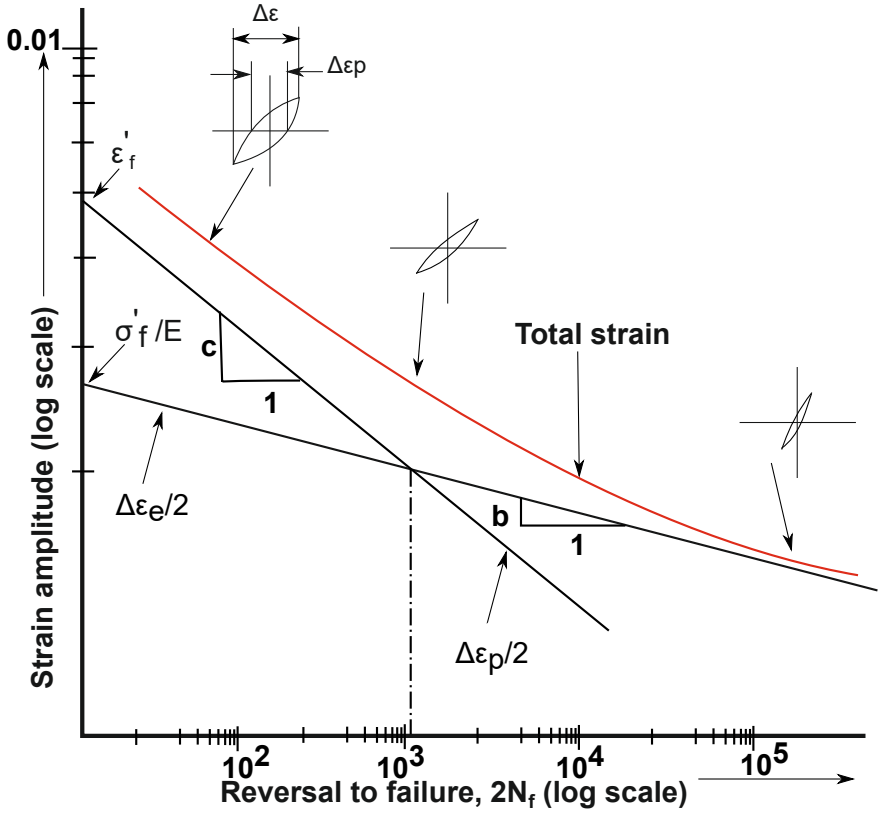

Figure 3.9: Strain-life (ε-N) fatigue curve [17]

The life at which elastic and plastic strain are equal the point is called as transition fatigue life which is represented by $2N_f$ as shown in the figure 3.9. Where the life below the transition life deformation is mainly plastic if the life above the transition life deformation is elastic, from this statement we can say that plastic deformation is present at even at relative at high cycles. This proves the accuracy of results in strain life method where in stress life fatigue method failed in giving the results of the plastic deformation in endurance limit[17, 10].

3.8 Transient cyclic response

During the cyclic loading material exhibit resistance to deformation, when the material is under fully reversed cyclic strain controlled loading. Material may behave as cyclic softening, cyclic hardening or remaining stable.

In cyclic hardening stress level at each successive strain reversal increases as number of cycle increases. On other hand cyclic softening is quit opposite to the cyclic hardening stress level at each successive strain reversal decreases as number of cycle increases. We can seen above phenomenons in the figures 3.10 3.11. But in both the phenomenon applied stress reduces and reach the steady state called as steady state response. This phenomenon is observed in the materials because of dislocation in crystal lattice of the material, for example soft materials like aluminum alloys with low dislocation tends to harden and hard materials like steel tends to soften [17].

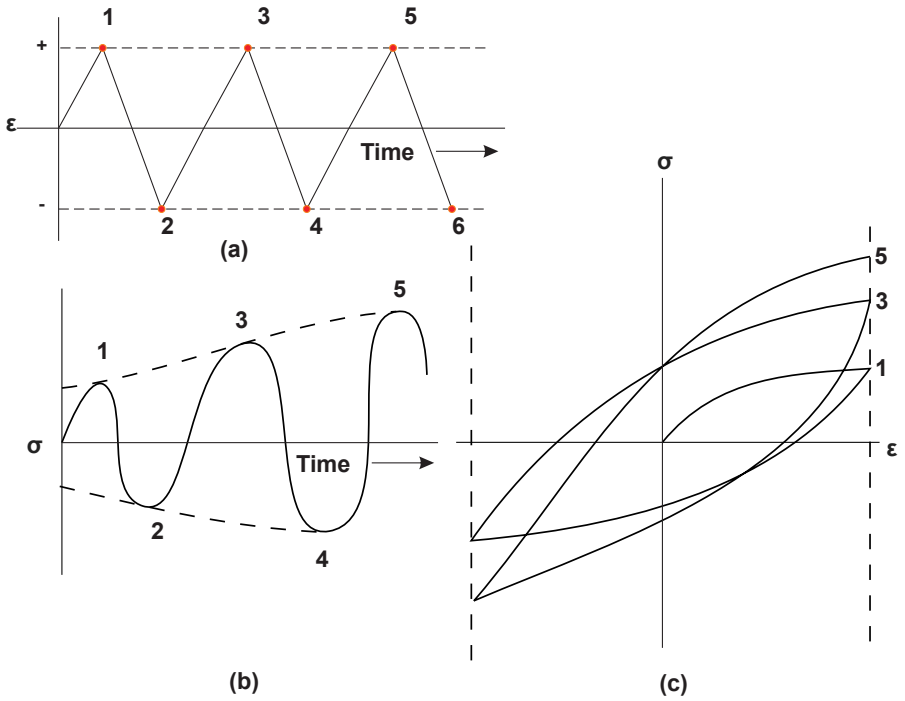

Figure 3.10: Cyclic hardening [10]

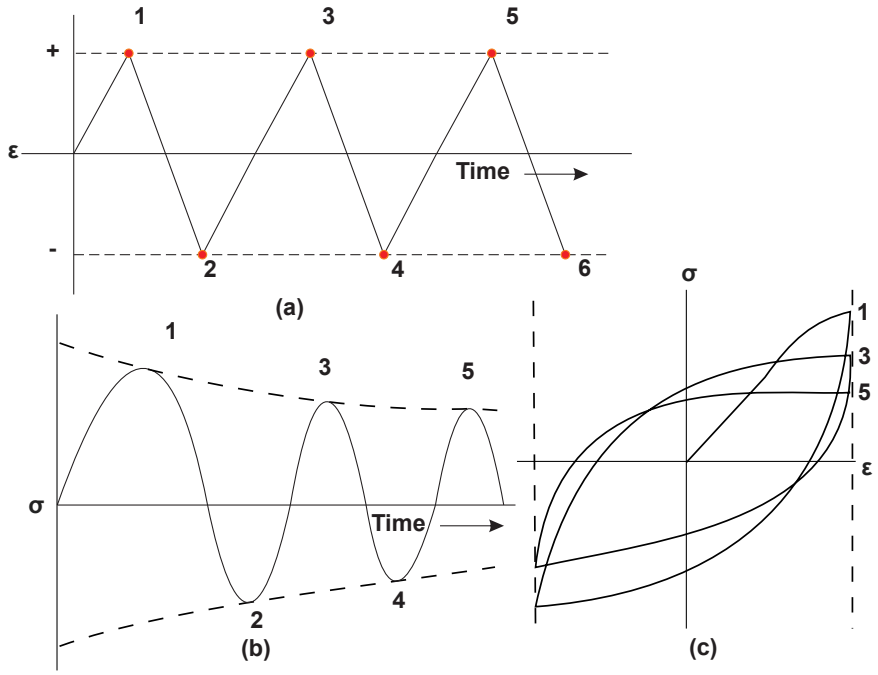

Figure 3.11: Cyclic softening[10]

4 H13 tool steel

4.1 Background of tooling materials

I strongly believe that every discovery starts with the need. If we look in the history need of strong materials for the weapons and tool, lead to the discovery of steels. The best early example is skill and knowledge of high strength steel in making swords produced in China. Officially the year 1740, is regard as the beginning of tool steels. when Benjamin and huntsman a clock maker from sheffeild, England melted piece of blister steel in crucible, which lead to the foundation of high performance steels. Crucible melting is continued to dominate making of tool steel until introduction of electrical furnace in 20^{th} century [13].

Properties of tool steel depends on the alloying element and heat treatment to obtain described properties. The understanding of corelation between carbon content, alloying composition and processing was known in 19^{th} century due to development in chemical analysis and metrology, which helped us to study the microstructure of tool steel. Alloying changed the development of tool steel. As discovery of chromium in 1797 R. A. Hadfield has investigated as an alloying element in steel give good hardness and toughness to steel. In the year 1868, Robert Mushet added tungsten to high carbon steel and it is regarded as first high speed steel [13].

In the year 1902, Otto Thallner mentioned in his book, that harness is associated with rapid cooling from the temperature little above the redness. Due to the Technological advancement in metalography, x-ray analysis, which allowed us for scientific understanding of phase transformation and micro structure of tool steels. During the period between 1920 to 1980, about 41 different high speed steel compositions have been discovered [13].

There are six groups in tool steels: water-hardened, cold-work, hot-work, high speed,shock-resistant,special purpose tool steels. As my thesis work is focused on H13 tool steel we will not discuss about other steels in literature [13].

4.2 Properties of H13 tool steel

H13 tool steel comes under hot-working group steels which are known as H steels. H13 tool steel is chromium based steel with 4.75 % to 5.50 % chromium. H13 tool steel has good temper resistance and maintain high hardness and strength at elevated temperature. It has good resistance to thermal fatigue, generally hot working tooling

are made from H13 tool steel and can be safely cooled between the operations. It also has good resistance to corrosion [2].

4.2.1 physical properties of H13 tool steel

Melting point and density of H13 tool steel are mentioned in the below table 4.1.

Properties	Metric
Density	$7.8\,g/cm^3$
Melting point	$1427\,°C$

Table 4.1: Physical properties of H13 tool steel[2]

4.2.2 Thermal Properties

Thermal properties of H13 tool steel like Thermal expansion and Thermal conductivity can be seen in the table 4.2

Properties	
Thermal expansion	10.4×10^{6} °C
Thermal conductivity	28.6 w/mk

Table 4.2: Thermal properties[2]

4.2.3 Annealing and Stress relieving

Annealing and stress reveling are important for the improvement of mechanical properties of the final product. Annealing and Stress relieving H13 tool steel are shown in the below points

- H13 tool steel is annealed at 871 °C and cooled slowly at 4 °C in furnace.
- H13 tool steel is heated to 700 ° c and cooled in air

4.2.4 Mechanical properties

Mechanical properties of H13 tool steel, oil quenched from 1010 °C and 2+2 hours at the indicated temperature. The test is done on at room temperature and the results are shown in the below table 4.3. Apart from the mechanical properties of H13 tool steel which is tested at room temperature, we can also see how the mechanical properties of H13 toll steel at different at different test temperatures and hardness which is shown in the below table 4.4 , Room temperature hardness HRC $52^{(a)}$ represent air cooled from 1010°c and doubled tempered, 2+2 h at the indicated temperature, $48^{(b)}$ hardness represent at the room temperature, $44^{(c)}$ hardness represent at 565°[2].

Tempering temperature °C	Tensile strength (Mpa)	yield Strength (Mpa)	Elongation in percentage	Reduction in area percentage
527	1960	1570	13.0	46.2
555	1835	1530	13.1	50.1
575	1730	1470	13.5	52.4
593	1580	1365	14.4	53.7

Table 4.3: Typical longitudinal room-temperature mechanical properties of H13 tool steel[2]

Room temperature hardness,HRC	Test temperature°C	Tensile strength (Mpa)	yield Strength (Mpa)	Elongation in percentage	Reduction in area percentage
52 [(a)]	425	1620	1240	13.7	50.6
	540	1305	1000	13.9	54.0
	595	1020	825	17.5	65.4
	650	450	340	28.9	88.9
48 [(b)]	425	1400	1150	15.0	59.9
	540	1160	960	17.1	62.4
	595	940	750	18.0	68.5
	650	455	350	33.6	89.0
44 [(c)]	425	1200	1005	17.0	64.1
	540	995	820	20.6	70.0
	595	827	690	22.6	74.0
	650	450	350	28.4	87.6

Table 4.4: Longitudinal short-time tensile properties of H13 tool steel[2]

4.3 Use of H13 tool steel in Additive Manufacturing

H13 tool steel is one of the most widely used metal for manufacturing the die casting and forging dies. The production of H13 in conventional method takes more time and material waste. In Additive manufacturing technologies we can overcome the problem material waste and design freedom, but H13 tool steel is very difficult to process using these technologies. In AM technologies high laser power and rapid cooling rate induces internal stress which leads to cracking of the part. In the article [6], cooling rate in DMS and SLM is around 270°C/s, which is fast and leads to the internal stress . In the same article they mentioned that, in SLM process they observed high tempering of under laying layers.we can see in figures 4.1 and 4.2 how the microstructure is varying in different layers. In general H13 tool steel can be easily quenched up to 120mm depth in still air.

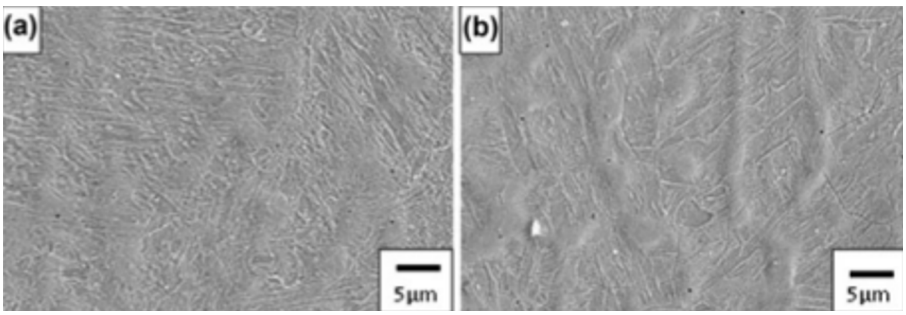

Figure 4.1: SEM view of first layer

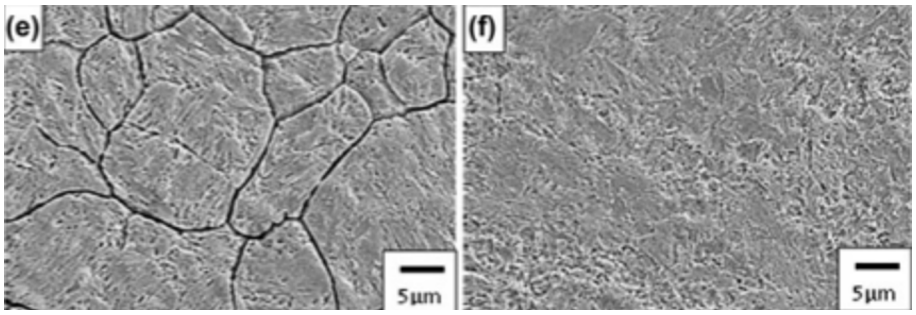

Figure 4.2: SEM view of fifth and sixth layer

The Microstructure and Hardness of H13 tool steel varies for different AM technologies. In SLM processthe hardness of H13 tool steel as–built part is 57 HRC and 48 HRC after annealing. In EBM process it was observed that hardness of as–bulit specimen is 48 to 50 HRC and 20 HRC after annealing, which was observed by [5]

4.4 Stress-life fatigue data of H13 tool steel

The below data on H13 tool steel stress life fatigue is taken from two different types ESR H13 and air melted H13 tool steel.

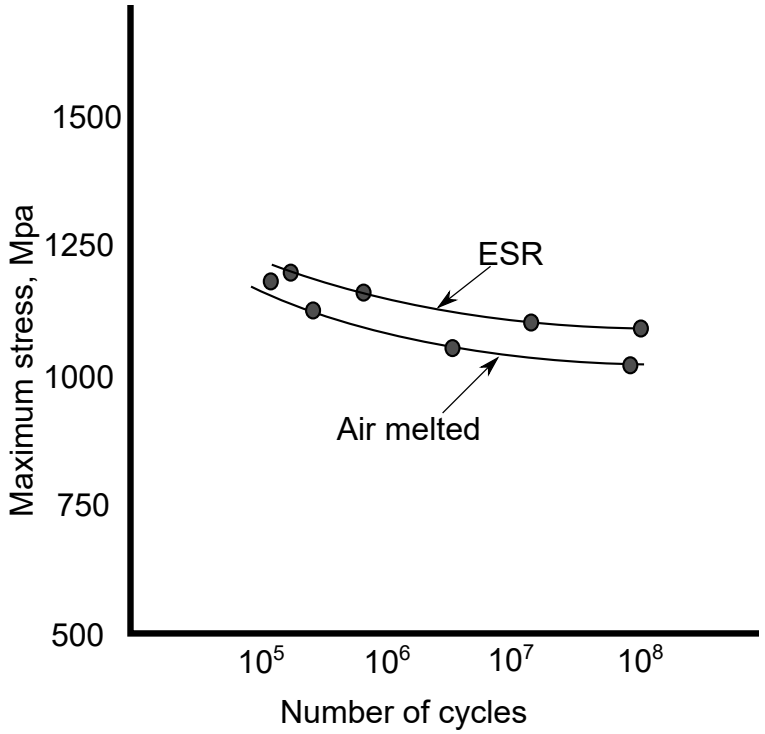

Figure 4.3: Tension tension fatigue curve for longitudinal specimen of air-melted and electroslag-remelted heats of H13 tool steel. test is carried with 60 HZ and alternating stress is 67 % of the mean stress(R=0.2) and the arrow in the graph says that without sign of fatigue cracking[2]

4.4.1 chemical composition of H13 tool steel used in SLM machine

The table 4.5 show the chemical composition of H13 tool steel powder used in selective laser melting technology.

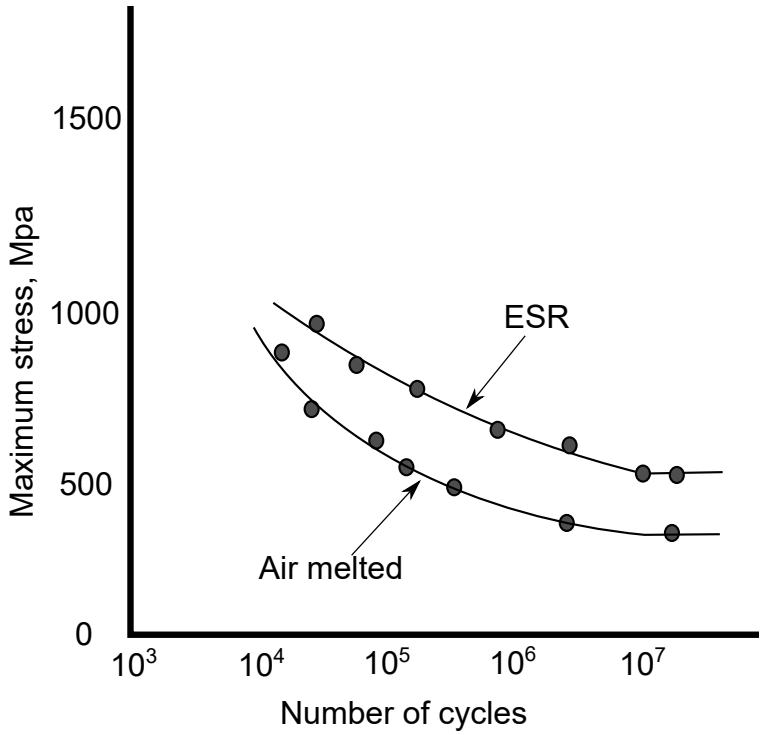

Figure 4.4: Tension-compression fatigue curve for air-melted and electroslag-remelted heats of H13 tool steel. Axial fatigue test performed with 60 Hz and R=-1[2]

Elements	H13 tool steel powder used in SLM	Conventional H13 tool steel
Iron (Fe%)	BAL	BAL
Carbon (C%)	0.42	0.32
Manganese (Mn%)	0.44	0.20
Silicon (Si%)	0.85	0.08
Sulfur (S%)	0.01	0.0
Phosphorus (p%)	0.01	0
Nickel (Ni%)	0.01	0
Chromium (Cr%)	5.22	4.75
Molybdenum (Mo%)	1.50	1.10
Copper (Cu%)	0.01	0
Vanadium (V%)	1.04	0.80
Niobium (Nb%)	<0.01	0
Titanium (Ti%)	0.01	0
Aluminum (Al%)	0.01	0

Table 4.5: Chemical composition of H 13 tool steel powder and conventional manufactured chemical composition

5 Microstrucure of the specimens

5.1 Fabrication of samples

All the samples for microstructure analysis were produced in the Laboratory of Rapid Prototyping at the The Institute for Nanomaterials, Advanced Technology and Innovation at Technical University of Liberec using SLM 280^{HL} machine from German manufacturer SLM Solutions AG (Figure 5.1).

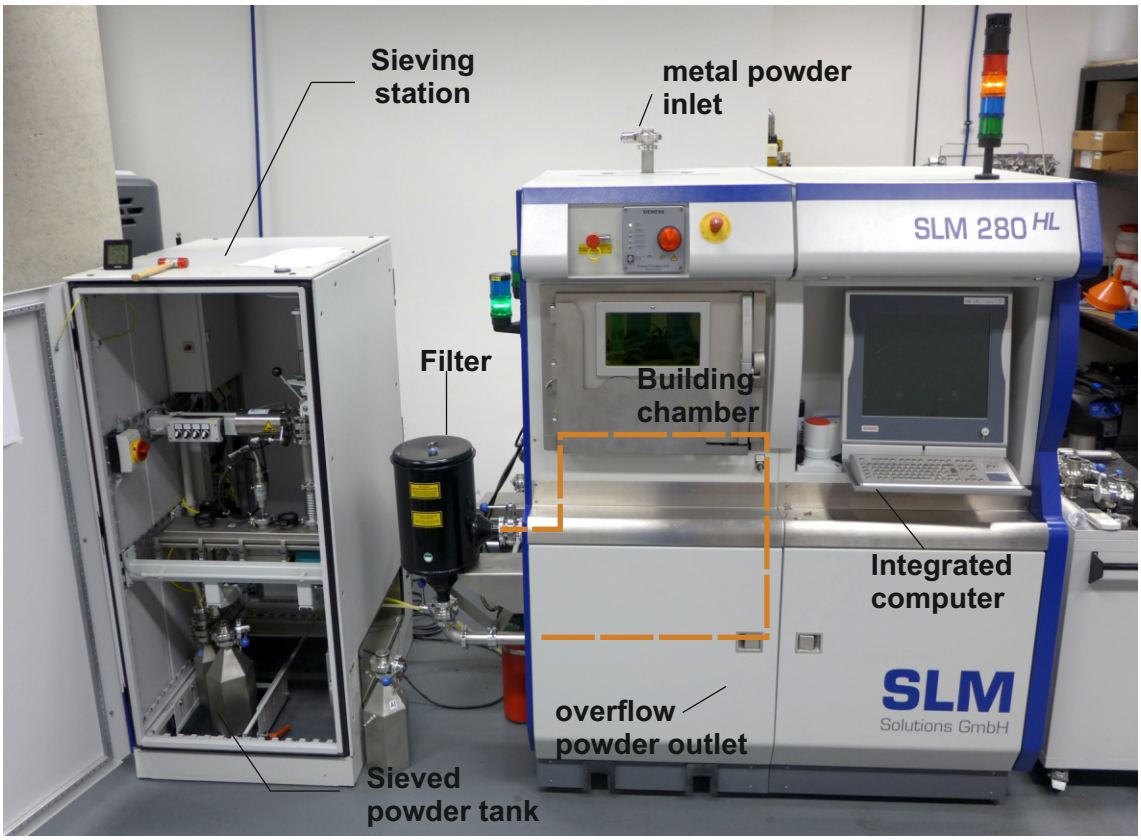

Figure 5.1: SLM 280HL printer (SLM Solutions AG)

The process in SLM 280^{HL} starts with placing the overflow powder tank in the sieving station for separating the unwanted powder particles. Sieving should be done under controlled level of oxygen in order to prevent the powder from explosion or fire.

After the sieving is done, tank in the bottom of the sieving station which contains the sieved powder is removed from the sieving station. The sieved powder tank is fixed to the metal powder inlet at the top of the machine and the empty tank in the sieving station is fixed to the overflow tank in machine.

The whole building process is governed by the machine computer integrated unit and fill the chamber with inert gas such as nitrogen (N_2) or Argon (Ar) in order to avoid the oxygen in the chamber. This is done using two integrated valves called gas inlet and gas outlet. The two valves are used to inlet the inert gas and to outlet the air from the building chamber. Oxygen level must be lower than 0.2 % to avoid the fire in the chamber during the building process. Base plate in the chamber should be adjusted parallel to the base of the chamber and fix it as 0 position. Then layer of powder should be spread over the base plate by recoter in order to check the equality of the layer deposition. Then the CAD stl format is imported to the machine for the building process. After the part is build the excess powder is removed and base plate is unscrewed from the chamber base. We can see the powder inlet, sieving station, building chamber, computer integrated system in the figure 5.1

5.1.1 Analysis of h13 powder particle size

H13 tool steel powder was provided by the SLM Solutions AG company together with data sheet. Given data sheet provides the information about the particle size distribution throughout whole package. The data sheet is useful for evaluation of powder quality and its applicability to SLM process. The machine which is used for the evaluation of the particle size is Cilas 990L, which is capable of measuring the particle size from 0.2-500 µm. Second observation for examination of particle shape was done using scanning electron microscope (figure 5.2). The histogram in the figure 5.3 shows distribution of the particle size.

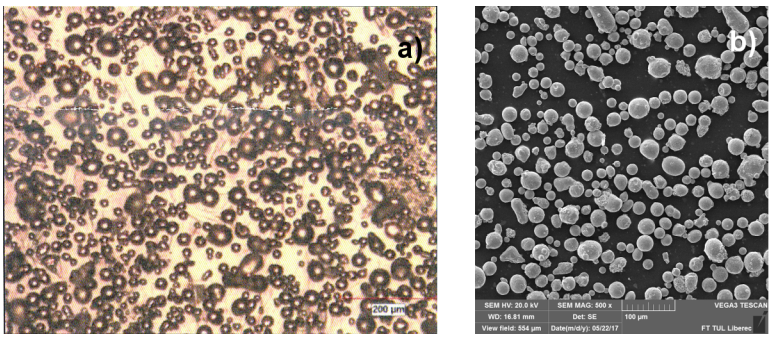

Figure 5.2: Shape and size analysis of H13 tool steel powder particles a) Cilas 990L analysis, b) SEM analysis

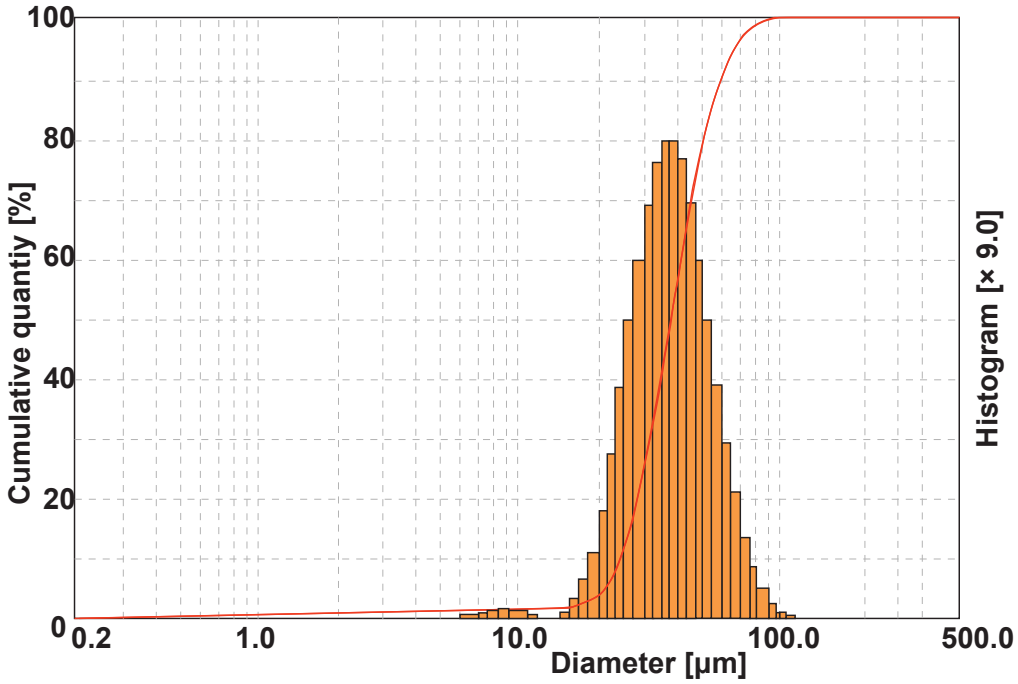

Figure 5.3: Particle size distribution

5.2 Preparation of samples

The below figure 5.4 and table 5.1 show parameters and vectors used for printing the specimen. In the figure 5.4 Border (A) is the shell of the specimen, which is process with low power and the scanning speed in order to obtain good surface finishing. Fill counter (B) which connects the Volume hatch (C) and Border (A). Volume hatch (C) or core which is processed with high scanning speed and power in order to build the specimen quickly and with sufficient density. Finally Vector support (D) which is processed with same power used for Border(A) and half the scanning speed used for the Core or Fill counter. The supports are very brittle in order to remove them easily from specimen.

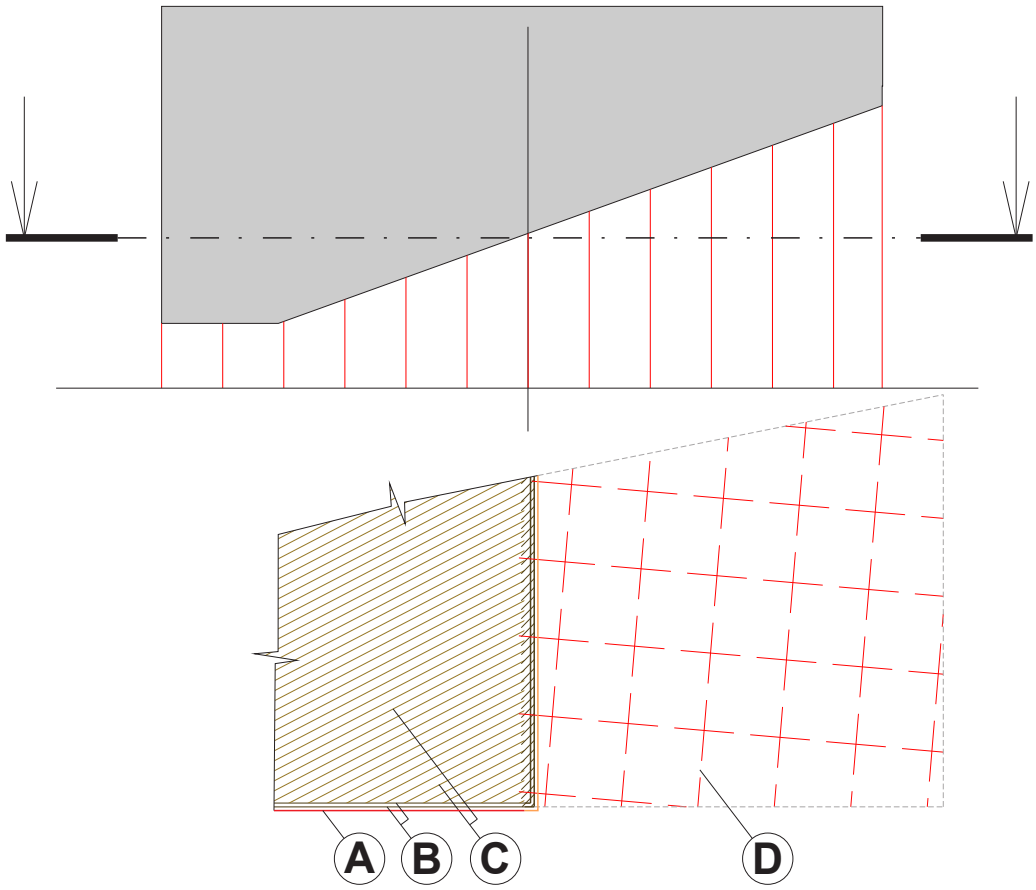

Figure 5.4: vectors used for the building stagy in SLM 280HL machine for $30\mu m$

Vector name	Border (A)	Fill contour (B)
Power P [W]	100	150
Scanning Speed v [mm/s]	470	525
Tracks	1	2
Hatch distance h [mm]	-	0.09
Rotation Angle [°]	-	
Vector name	Volume hatches (C)	Vector Support (D)
Power P [W]	350	100
Scanning speed v [mm/s]	1400	700
Tracks		
Hatch distance h [mm]	0.12	
Rotation Angle [°]	90 °	

Table 5.1: SLM 280HL machine parameters for H13 tool steel

5.3 H13 Microstructure Analysis

In order to evaluate microstructure of the specimens, number of various test were performed. The work and results were done in cooperation with COMTES FHT company (Dobřany, Czech Republic). For the tests, two samples built under same building parameters were submitted. First of the two samples is in as–build condition. Second sample was heat treated in order to remove the internal stress. The stress relief annealing is done at the end of each building job in the Laboratory of Rapid Prototyping and it contains heating the part up to 620°C and sustaining at this temperature for 2 hours. Then, the part is cooled down naturally in the oven and after reaching 100°C it is cooled down in still air.

5.3.1 Preparation of samples

The printed samples in the form of simple cube with edge length of 10 mm were cut in two planes – vertically and horizontally with respect to original building direction. Overview of cutting planes are shown in the figure 5.5.

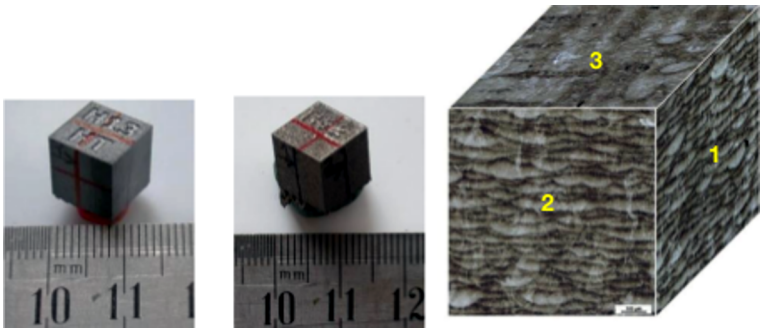

Figure 5.5: Form of the specimen and cut planes; 1,2-perpendicular to build direction; 3-parallel with building direction

5.3.2 Microstrucure analysis

Microstructure of the specimen was developed using Villela-Bain and Glyceregia chemical agents. With using this approach it was possible to analyse the mirostructure using optical microscope Carl Zeiss AXIO Observer.Z1m. Microstructure of the samples was also analyzed using scanning electron microscope Jeol JSM 6380.

In the figure 5.6, results from the optical microscope can be seen on the plane perpendicular to the building direction. We can clearly see the traces of individual melt pools in several layers. In greater magnification which was done using SEM, the type of the structure can be recognized. The as–built specimen is formed of mix of martenstic structure and tempered martensite (figure 5.7). Final structure in the specimen is most probably caused due to the combination of material properties and SLM process. Fast melting and solidification of the powder leads to influencing

not the actually processed layer but also the underlying volume of the built part. Such process leads to introduction of high internal stresses and possibility of cracks formation.

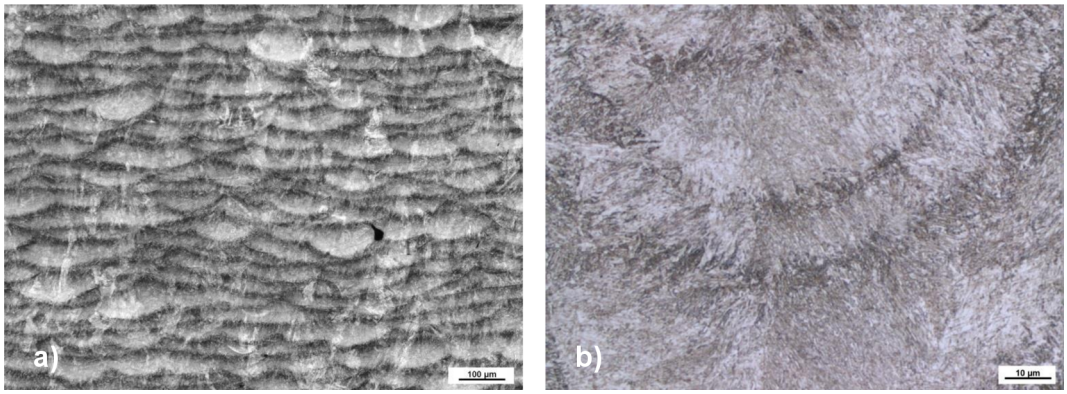

Figure 5.6: View of microstructure, as built specimen (a)100x and (b) 1000x

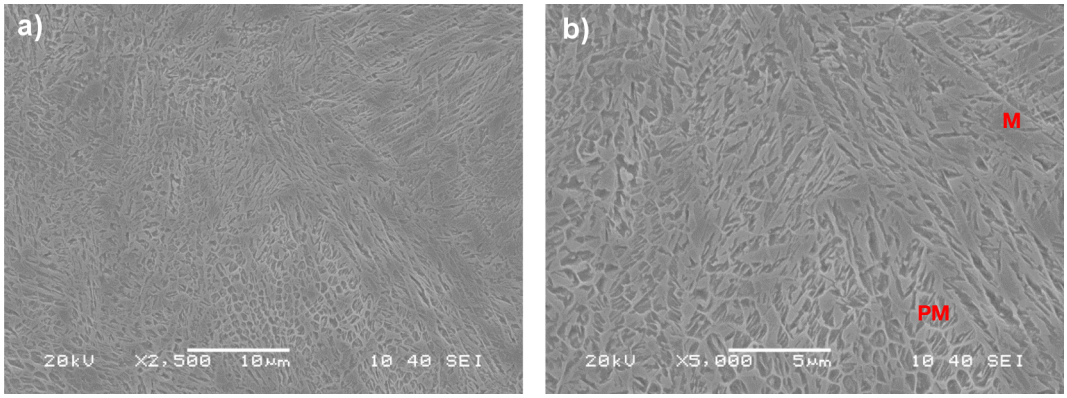

Figure 5.7: View of microstructure, as built specimen (a) 2500x and (b) 5000x

In the two figures 5.8 and 5.9 the microstructure of the specimen after stress relief heat treatment is displayed. From the optical measurement (5.8) we can observe that the melt pool boundaries which were seen in the as–built condition 5.6 were suppressed. Following SEM analysis revealed the fact that the microstructure of the specimen is homogenous and it is formed out of tempered martensite.

Observation of the microstructure on the plane parallel to building direction is enclosed in appendix B.

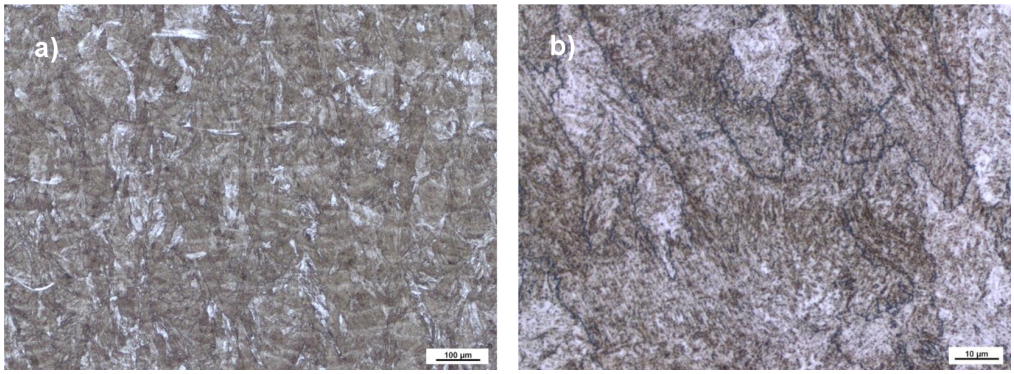

Figure 5.8: View of microstructure, annealed specimen (a)100x and (b) 1000x

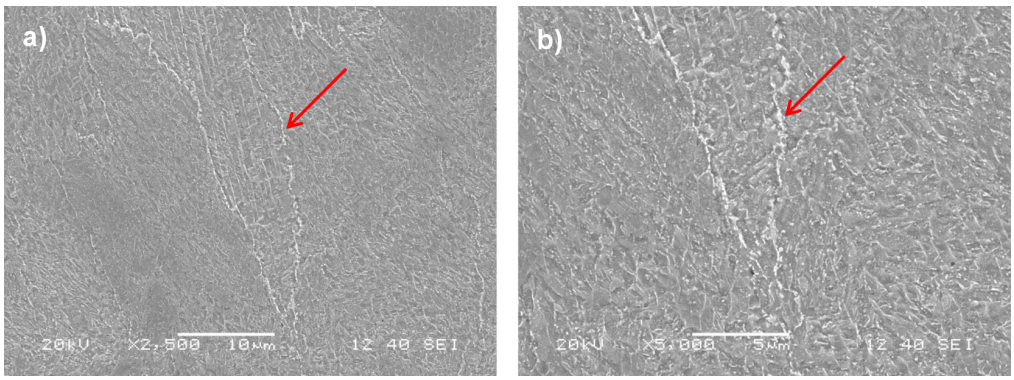

Figure 5.9: View of microstructure, annealed specimen (a) 2500x and (b) 5000x

5.3.3 porosity

Porosity of the specimens was evaluated using analysis of the image (figure 5.10). Results of the analysis on all three planes are summarized in table 5.2.

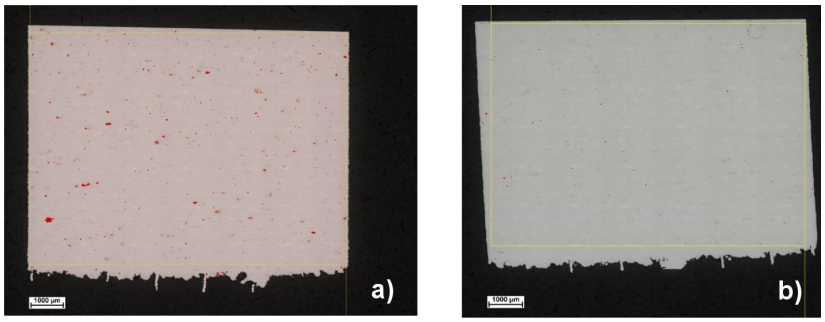

Figure 5.10: View of porosity, annealed specimen (a) 2500x and (b) 5000x

Samples	Porosity [%]	Maximum Size of Pore
H13-1	0.17	233.9
H13-2	0.11	197.1
H13-3	0.12	264.9
H13-HT-1	0.01	43.5
H13-HT-2	0.01	43.2
H13-HT-3	0.02	34.6

Table 5.2: Porosity of H13 tool steel

5.3.4 Hardness

Vickers hardness measurement was done with use of STRUERS DuraScan machine for both as-built and heat treated specimen. Data were then also converted to Rockwell hardness (table 5.3).

Hardness	H13 as built	H13 heat treated
Vickers Hardness (HV)	624	494
Rockwell C Hardness (HRC)	57	49

Table 5.3: Hardness test results of H13 tool steel processed by SLM Technology

6 Mechanical testing

Main aim of this work is evaluation of strain-life data of SLM-printed parts from H13 tool steel. For this purpose, ASTM E606-12 standard was used as a guidance for proper settings of the test and fabrication of the samples with standardized shape. Although quasi-static properties of H13 tool steel were studied in the previous work of the laboratory, it was decided to repeat it on one ASTM specimen for verification and convenient setting of strain amplitudes.

6.1 Fabrication of specimens

Figure 6.1 shows form of the specimen used for strain-life fatigue testing. Complete drawing of the specimen which includes the tolerances of the part and its surface finish can be found in the appendix. Generally, the demand on shape precision and quality of specimen's surface is much higher for fatigue tests than for the specimens for tensile testing. Chosen shape of the specimen was created in PTC/Creo with 0.2 mm surface offset because of further grinding and other finishing operations.

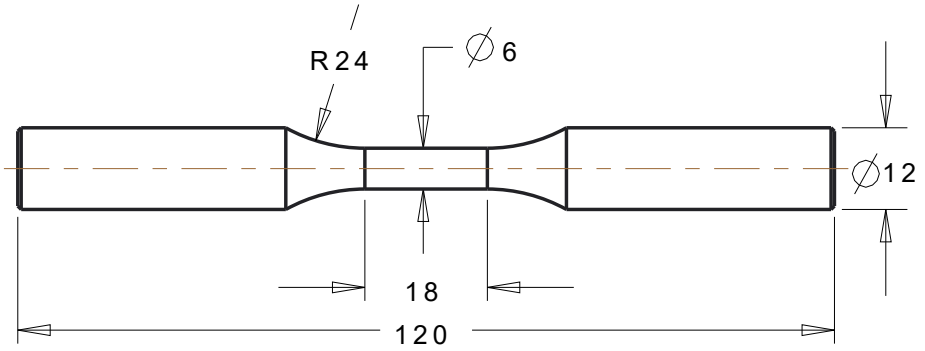

Figure 6.1: Dimensions of the test specimen with Standard E606

In the preprocessing part of the print, Materialise Magics 21 was used for data handling. CAD model of the specimen was translated to STL format and positioned in the upright orientation relatively to the building platform. Support structures were needed only on the bottom side of the part. During one job, 60 samples were printed (Figure 6.2) under the same building strategy as described in previous chapter. Using the 30 µm layer thickness, the given build job took 5 days and 13 hours

to finish. Half of the final amount was removed from the substrate plate after finishing and second half was submitted to stress relief annealing (the heat treatment procedure is described in section 5.3).

Figure 6.2: ASTM E606 specimens after print on SLM 280^{HL}

6.2 Tensile Test

Tensile test is one of the most basic measure to evaluate the mechanical properties of the materials. In the case of following strain-life fatigue tests, it is necessary to study quasi-static properties of the material for proper setting of the testing method. The test procedure is very simple and inexpensive. It starts with fixing the specimen in the upper and lower jaw of the tensile test machine and applying the tensile load on the specimen until it breaks. The reason for applying the load is to know how the material react to the load. During the test, we obtain the relation between force F and elongation Δl of the specimen. After the data are transferred to stress-strain coordinates, basic mechanical properties such as Young's modulus E, Yield strength R_e and Ultimate tensile strength R_m can be determined.

6.2.1 Testing method

Tensile test was carried out on INOVA FU-O-160-1600-V2 servohydraulic testing machine which is situated in the Laboratory of Progressive Industrial Technologies, CxI at Technical University of Liberec. The machine is primarily used for cyclic testing and it is equipped with axial motor having the loading capacity of $\pm 100\,\mathrm{kN}$

and torsional motor with loading capacity of ±200 Nm. Thus, the machine is capable to perform combined tension/torque cyclic tests.

As an optional equipment, the machine is also provided with EPSILON TECH 3442 extensometer for proper measurement of elongation at specimen's reduced area. The extensometer has 12.5 mm initial length between its fastening blades and according to the test certificate which is provided by the manufacturer, it fits into the B-1 precision class with respect to ASTM E83 standard.

After fastening the specimens into hydraulic clamps of the machine, 1 kN pretension was applied to the specimen for preventing any sliding and clearance in clamping. In this stage, the extensometer was fastened to reduced section of the specimen 6.3 and its signal was compensated to zero value. Tensile test was then done under position control with load rate of 1 mm/min until rupture. During the test, elongation data were recorded from extensometer together with the force feedback from the load transducer.

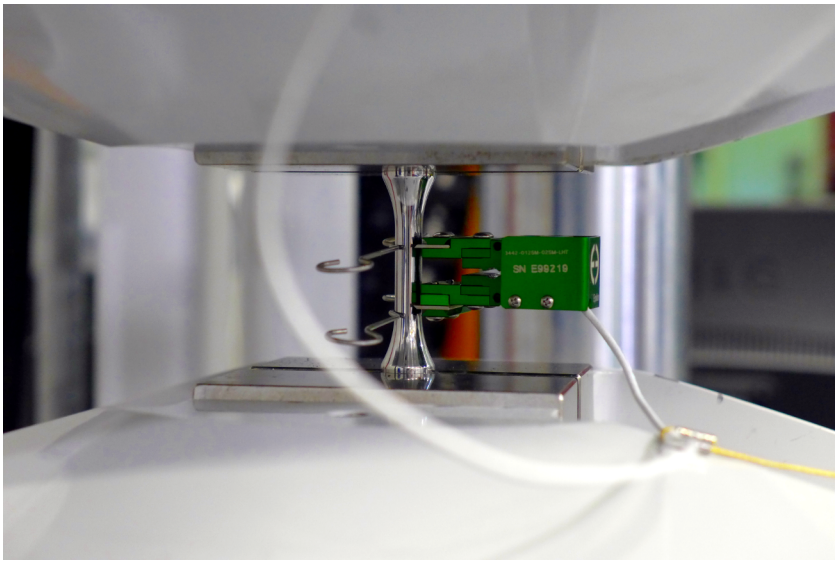

Figure 6.3: Specimen and extensometer arrangement

6.2.2 Results

In the post-processing part of the test, the data gained from the measurement were transferred to engineering stress-strain space (Eq. 6.1 and 6.2). Graphical representation of tensile test data for the studied material is displayed in figure 6.4.

$$\sigma = \frac{F}{S_0} \qquad (6.1) \qquad\qquad \varepsilon = \frac{\Delta l}{l_0} \qquad (6.2)$$

As it can be seen in the figure 6.4, the material is very brittle even after heat treatment. Tensile curve up to its ultimate tensile strength is smooth without distinct

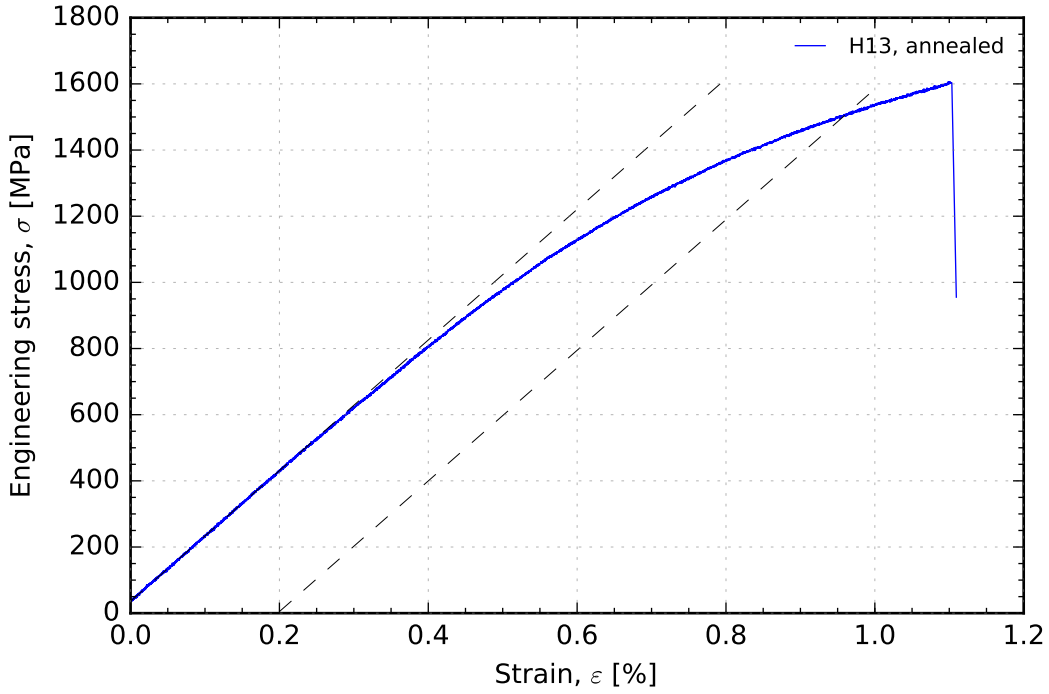

Figure 6.4: Stress-strain curve of H13 tool steel

yielding point and thus it is only possible to evaluate 0.2% offset yield stress. With using the linear fit of the initial part of the stress-strain diagram, it was possible to evaluate basic mechanical properties of the tested material. All the calculated values are summarized in the table 6.1.

Ultimate tensile stress	R_m	1600 MPa
Strain at break	ε_b	1,1%
Offset yield stress	$R_{e0.2}$	1510 MPa
Young's modulus of elasticity	E	197,000 MPa

Table 6.1: SLM-printed H13 tool steel tensile properties

6.3 Strain-life fatigue test

6.3.1 Specimen surface roughness

As discussed in the previous sections, surface finish of the specimen is a vital parameter for convenient evaluation of fatigue life. Any kind of notch, even the marks from grinding operations result in shortening of life due to easier initiation of the crack. In our case, the thin part of fatigue specimens is prescribed to be polished

to mean roughness of 0.2 µm. It was decided to verify the finish with use of Bruker DektakXT profilometer (figure A.2).

Bruker machine is used for measuring the surface texture with high accuracy. Important aspect in this machine is stylus or probe which runs over the surface of the sample beneath it. Depending on the application, there are different types of stylus shape and size. The specimen was attached to the base plate of the machine using clay as shown in the figure 6.5. Surface measurement was performed with use of 2 µm stylus and measuring speed of 150 µm/s over the track 10 mm i length. The results of the surface roughness of the specimen are showed in the figure 6.6 and they clearly confirm desired value of specimen surface roughness of 0,2 µm.

Figure 6.5: Arrangement of specimen in the Bruker machine

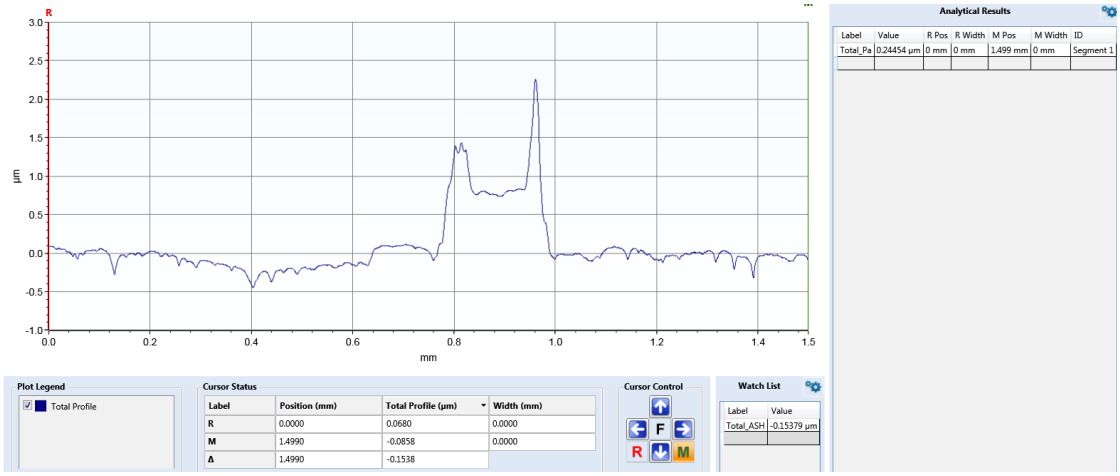

Figure 6.6: Results of the surface roughness measurement

6.3.2 Testing method

For the strain-life fatigue testing, same machine and equipment was used as described in previous section. Testing method was set in such a way to evaluate both low and high cycle fatigue part using fully reversed cycle with $R = -1$ under testing frequency of 1 Hz. According to the ASTM standard, it is common to use 18 specimens for evaluation of the ε-N curve. In our case, three samples were tested for the same level of strain amplitude.

The testing method was carried out using the following procedure:

1. Clamping of the specimen into hydraulic clamps with compensation of force for preventing damage of specimen
2. Ramp to zero value of force
3. Fastening of extensometer
4. Change of driving feedback to extensometer signal
5. Submission of cyclic test at selected strain amplitude

6.3.3 Results

All the results are summarized in table 6.2. Value of elastic strain amplitude was determined from steady-state hysteresis loop which was recorded throughout the test. Using the least square method for fitting the approximation curve (equation 3.7), it was possible to evaluate fatigue strength coefficient $\sigma_f^{'}$ and fatigue strength exponent b from elastic strain data. Value of plastic strain amplitude was then calculated by subtracting of elastic strain amplitude from value of total strain amplitude. With fitting the curve according to Manson-Coffin relation (equation 3.8) to plastic strain we finally obtain fatigue ductility coefficient $\varepsilon_f^{'}$ and fatigue ductility exponent c (table 6.3)

Graphical representation of the data is shown in the figure 6.7. As it can be seen, there is very small contribution of plastic strain to fatigue damage of the material. This feature can be addressed to microstructure of the specimen, formed of very hard and brittle tempered martensite. The hysteresis loop was very narrow during the test even at low cycle fatigue region.

6.3.4 Study of specimen fracture surface

One of the samples was subjected to evaluation of fracture surface with use of Carl Zeiss AXIO Imager.Z2 optical microscope. In the figure 6.8, the fracture surface of the specimen tested at 0.008 total strain apmitude is displayed in 50x magnification. Thanks to this magnification it is possible to observe the whole cross-sectional area. Fracture initiation and propagation site can be distinguished thanks to distinct border with brittle fracture area caused by overload of the remaining cross-section.

Strain Amplitude	Reversals to failure	Elastic strain	Plastic strain
0.016	265	0.0158	0.0002
0.016	195	0.0159	0.0001
0.016	211	0.016	0.0
0.006	5000000	0.0056	0.0004
0.006	5000000	0.0059	0.0001
0.007	829125	0.0069	0.0001
0.007	912364	0.007	0.0
0.007	1135468	0.007	0.0
0.010	14326	0.009	0.001
0.010	15329	0.010	0.0
0.010	16257	0.010	0.0
0.008	430216	0.0077	0.0001
0.008	409452	0.0079	0.0001
0.008	583168	0.0079	0.0003
0.013	915	0.0129	0.0001
0.013	1011	0.013	0.0
0.013	1032	0.013	0.0

Table 6.2: Results of strain-life fatigue tests

Fatigue Strength Coefficient	$\sigma_f^{'}$	5120
Fatigue strength exponent	b	-0.09153
Fatigue ductility Coefficient	$\epsilon_f^{'}$	0.04192
Fatigue ductility exponent	c	-0.58631

Table 6.3: Strain-life constants for H13 tool steel

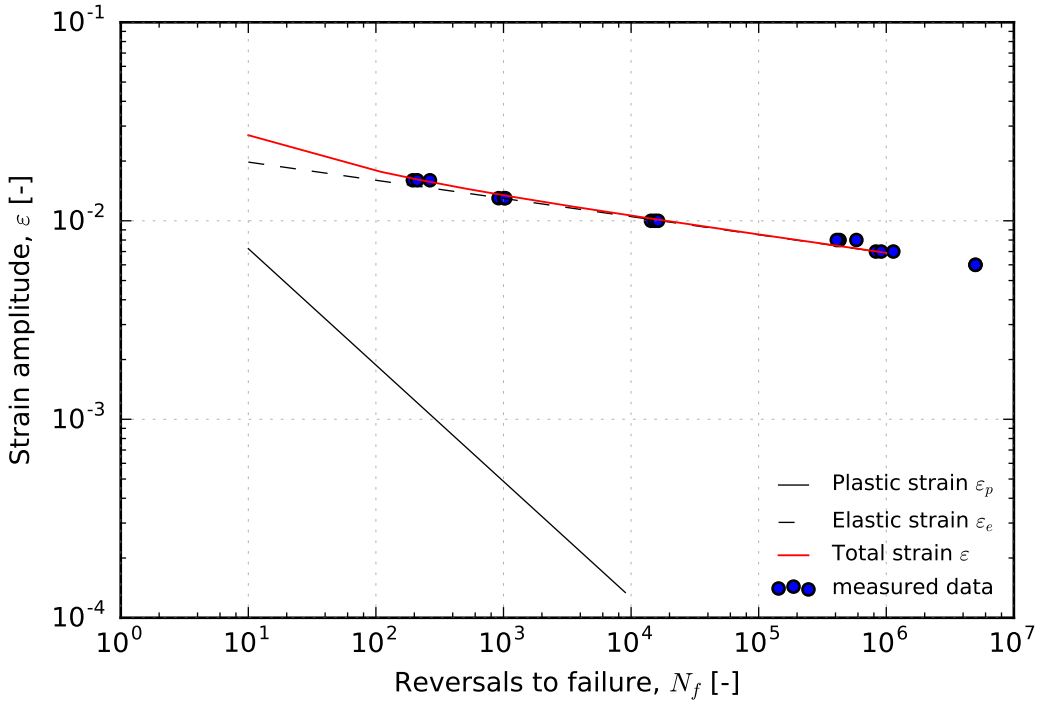

Figure 6.7: Strain-life curve of H13 tool steel

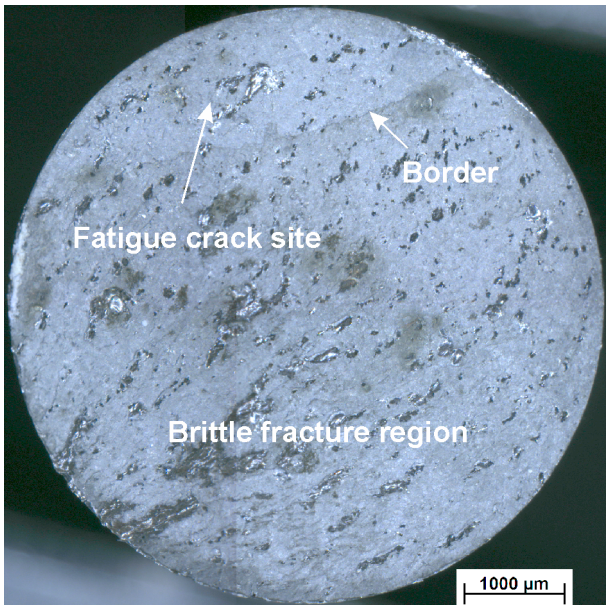

Figure 6.8: Specimen fracture surface

7 Discussion

Processing of H13 tool steel using Selective Laser Melting is a very complex problem. As it can be seen from the results of microstructure, fast cooling and subsequent solidification of the material which takes place almost in single point of the building area introduces large internal stresses to the parts which eventually leads to crack formation at both micro- and macroscopic level.

Examination of SLM-processed H13 tool steel under optical and scanning electron microscopes lead to the finding that the microstructure of the as-built specimens is composed of mix of martensite and tempered martensite. Such a structure is most probably caused by the fact that underlying material is influenced by ongoing SLM process of the current layer. Standard heat treating process which is used in Laboratory of Rapid Prototyping at TU Liberec after each building job leads to homogenization of the structure and suppression of melt pool traces. The hardness of the material is also lowered thanks to heat treatment. Unfortunately, stress relief heat treatment can be used at present state only as a post-processing operation. This fact puts a great demand on supporting structures of the models which, as a consequence, has to be very rigid and they are hard to be removed after the build.

Mechanical testing was carried out on heat treated specimens only due to lack of time and frequent malfunction of the cyclic testing machine. Tensile test verified consistency of mechanical properties in comparison with previous work of the Laboratory [14]. Final stress-strain curve is smooth without distinct yielding limit.

Fatigue testing of the material, which was main motivation of my thesis, brought new insight into the material behavior under cyclic loading. Chosen strain-life approach had its limitations – especially in the demands to precision of the extensometer and proper driving of the test via INOVA TestControl software. Due to its brittleness, the material shows low resistance to fatigue under fully reversed cycling. Analysis of the steady-state hysteresis loop shows that plastic deformation contributes fatigue failure only in the very limited portion. For H13 tool steel, only limited information about its strain-life data is available. The only comparison of the data can be then made with available S-N data for H13 tool steel or ε-N data for similar materials. With respect to data provided by ASTM hanbook (figure 4.4), fatigue limit of conventional H13 tool steel was determined to approx 400 MPa under fully reversed loading. In our tests, the load response during the lowest strain amplitude of 0.006 in which there is no plasticity contribution was 3,54 kN. This load corresponds to value of 127 MPa when calculated via measured cross-section of the specimen. Concerning comparison with similar materials, Liu et al. [11] performed strain-life fatigue testing on DIN 1.2367 tool steel under various heat treatments.

Our data are comparable to those published in their article especially in the case of low fatigue resistance and determined value of related Basquin's and Manson-Coffin's constants. With respect to this reference, we can expect our values to be valid and that main goal of the thesis was fulfilled.

8 Conclusion and further work

This master thesis brought wider information about processing of H13 tool steel with use of Selective laser melting technology. Main contribution of the work can be summarized into following three points:

1. Study of microstructure revealed that large inner stresses observed during processing of H13 tool steel are most probably caused by influencing of underlying volume of the part due to ongoing SLM process.

2. Fatigue resistance of SLM-printed H13 tool steel is lower than in the case of conventionally processed material. This fact may be caused by final very hard and brittle inner structure.

3. Strain-life fatigue data shows that absolutely minor contribution of plastic strain is present even at testing total strains, corresponding to lowest levels of fatigue life

Due to time limitations it was not possible perform the fatigue tests on as-built specimens which were fabricated for theme of this thesis. This work will be then dealt with in upcoming months. Another field of interest is deeper study of the reason why is H13 tool steel liable to occurrence of cracks and distortions during SLM process.

Bibliography

[1] Agerskov, H. Fatigue in steel structures under random loading. *Journal of Constructional Steel Research 53*, 3 (2000), 283–305.

[2] ASM International. Handbook Committee. *Properties and Selection–Irons, Steels, and High-performance Alloys*. No. v. 10, no. 1 in ASM handbook. ASM International, 1990.

[3] Bhat, S., and Patibandla, R. *Metal Fatigue and Basic Theoretical Models: A Review*. INTECH, 2011.

[4] Campbell, F. C. *Elements of metallurgy and engineering alloys*. ASM International, 2008.

[5] Cormier, D., Harrysson, O., and West, H. Characterization of h13 steel produced via electron beam melting. *Rapid Prototyping Journal 10*, 1 (2004), 35–41.

[6] Cottam, R., Wang, J., and Luzin, V. Characterization of microstructure and residual stress in a 3d h13 tool steel component produced by additive manufacturing. *Journal of Materials Research 29*, 17 (2014), 1978–1986.

[7] Hanzl, P., Zetek, M., Bakša, T., and Kroupa, T. The influence of processing parameters on the mechanical properties of slm parts. *Procedia Engineering 100* (2015), 1405–1413.

[8] Kempen, K., Thijs, L., Vrancken, B., Buls, S., Van Humbeeck, J., and Kruth, J. Producing crack-free, high density m2 hss parts by selective laser melting: pre-heating the baseplate. In *Proceedings of the 24th international solid freeform fabrication symposium. Laboratory for freeform fabrication, Austin, TX* (2013), pp. 131–139.

[9] Kruth, J.-P., Froyen, L., Van Vaerenbergh, J., Mercelis, P., Rombouts, M., and Lauwers, B. Selective laser melting of iron-based powder. *Journal of Materials Processing Technology 149*, 1 (2004), 616–622.

[10] Lee, Y. *Fatigue Testing and Analysis: Theory and Practice*. Fatigue testing and analysis:. Elsevier Butterworth-Heinemann, 2005.

[11] Liu, C., Wu, J., and Kuo, C. Low-cycle fatigue of din 1.2367 steels in various treatments. In *Fracture of Nano and Engineering Materials and Structures*. Springer, 2006, pp. 217–218.

[12] Mazur, M., Mazur, M., Leary, M., Leary, M., McMillan, M., McMillan, M., Elambasseril, J., Elambasseril, J., Brandt, M., and Brandt, M. Slm additive manufacture of h13 tool steel with conformal cooling and structural lattices. *Rapid Prototyping Journal 22*, 3 (2016), 504–518.

[13] Roberts, G., Kennedy, R., and Krauss, G. *Tool Steels, 5th Edition:*. EngineeringPro collection. ASM International, 1998.

[14] Šafka, J., Ackermann, M., and Voleskỳ, L. Structural properties of h13 tool steel parts produced with use of selective laser melting technology. In *Journal of Physics: Conference Series* (2016), vol. 709, IOP Publishing, p. 012004.

[15] Sidambe, A. T. Biocompatibility of advanced manufactured titanium implants—a review. *Materials 7*, 12 (2014), 8168–8188.

[16] Spears, T. G., and Gold, S. A. In-process sensing in selective laser melting (slm) additive manufacturing. *Integrating Materials and Manufacturing Innovation 5*, 1 (2016), 1.

[17] Stephens, R., Fatemi, A., Stephens, R., and Fuchs, H. *Metal Fatigue in Engineering*. A Wiley-Interscience publication. John Wiley & Sons, 2000.

[18] Vrancken, B., Wauthlé, R., Kruth, J.-P., and Van Humbeeck, J. Study of the influence of material properties on residual stress in selective laser melting. In *Proceedings of the solid freeform fabrication symposium* (2013), pp. 1–15.

[19] Wohlers, T., and Gornet, T. History of additive manufacturing. *Wohlers Report: Additive Manufacturing and 3D Printing State of the Industry Annual Worldwide Progress Report* (2011).

A Machines used in the work

Figure A.1: INOVA cyclic testing machine

Figure A.2: Bruker surface roughness measuring machine

B Microstructure; parallel surface

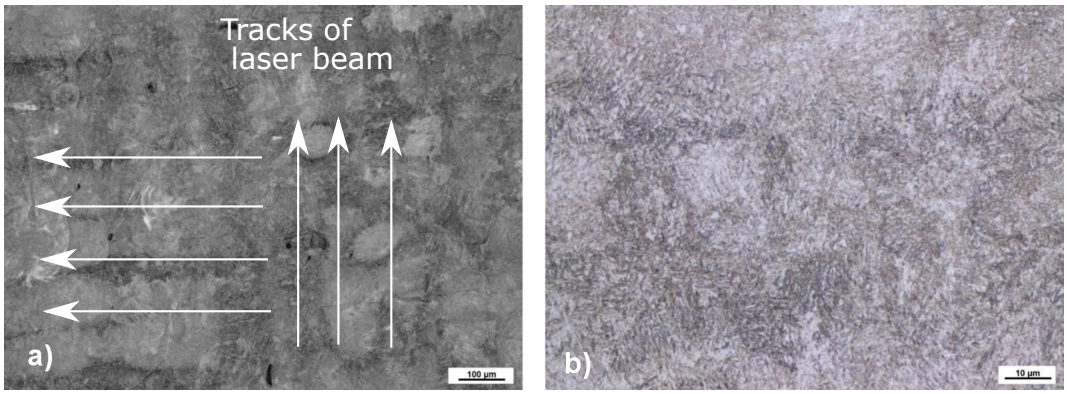

Figure B.1: View of microstructure on parallel surface, as built specimen (a)100x and (b) 1000x

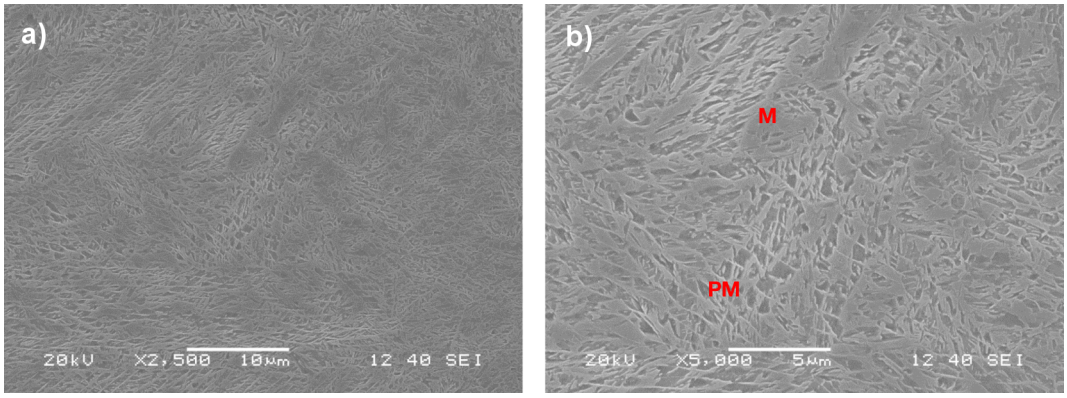

Figure B.2: View of microstructure on parallel surface, as built specimen (a) 2500x and (b) 5000x

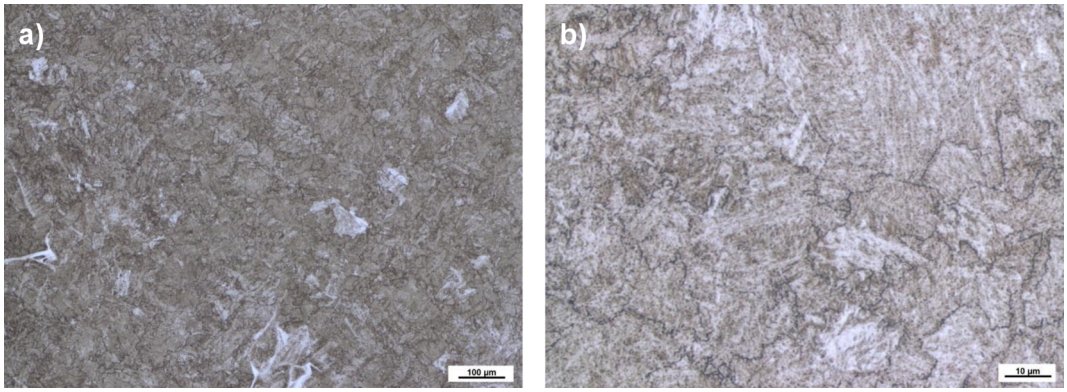

Figure B.3: View of microstructure on parallel surface, annealed specimen (a)100x and (b) 1000x

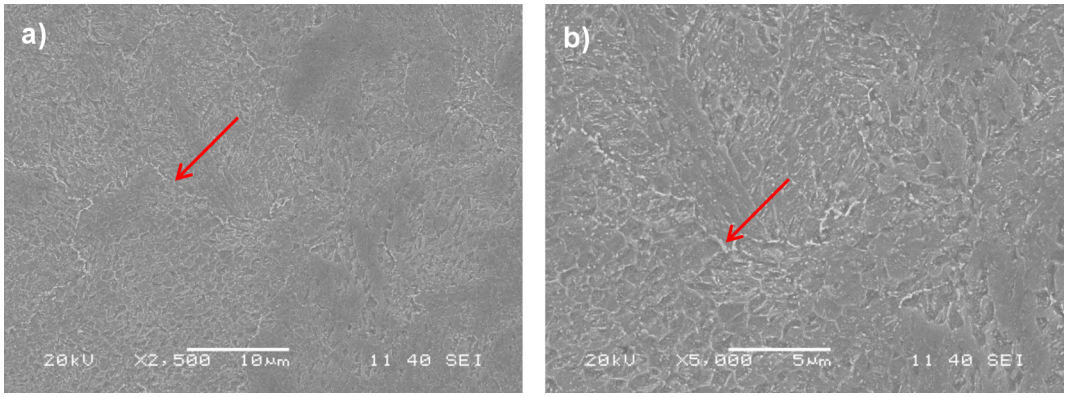

Figure B.4: View of microstructure on parallel surface, annealed specimen (a) 2500x and (b) 5000x

3.2

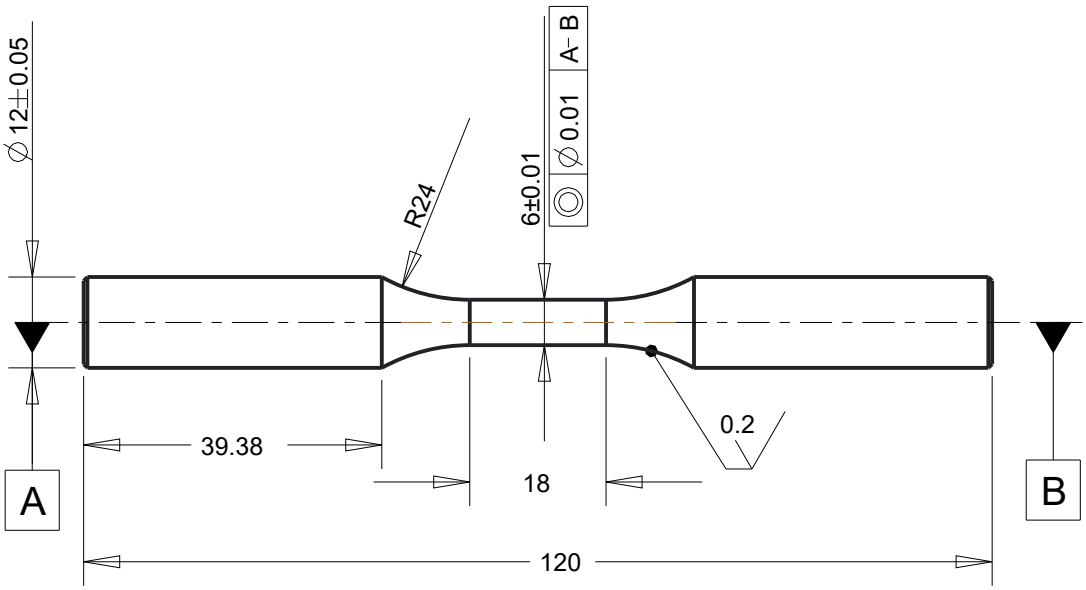

Roz. -Polot.							Presnost
		c)		Mater.		Tr. odp	Tolerovani
		b)		C. hm		Hr. hm.	
		a)					
Zmena	Datum	Index	Podpisy				
Meritko 1.000	Pozn.	Navrhl		TECHNICKÁ UNIVERZITA V LIBERCI www.tul.cz			
		Kreslil					
		Prezkousel		Nazev	4-KAS-VASTA-00-01		
C. seznamu		Technolog					
C. sestavy		Normaliz.		Cis. vykresu			
Stary vykr.		Schvalil					
Novy vykr.		Datum	May-22-17	list 1 listu1			